

Integrative Clustering of Multi-View Data by Nonnegative Matrix Factorization

Shuo Shuo Liu

SHUOSHUO.LIU@PSU.EDU

Lin Lin

LLIN@PSU.EDU

*Department of Statistics
The Pennsylvania State University
University Park, PA 16802, USA*

Abstract

Learning multi-view data is an emerging problem in machine learning research, and nonnegative matrix factorization (NMF) is a popular dimensionality-reduction method for integrating information from multiple views. These views often provide not only consensus but also diverse information. However, most multi-view NMF algorithms assign equal weight to each view or tune the weight via line search empirically, which can be computationally expensive or infeasible without any prior knowledge of the views. In this paper, we propose a weighted multi-view NMF (WM-NMF) algorithm. In particular, we aim to address the critical technical gap, which is to learn both view-specific and observation-specific weights to quantify each view's information content. The introduced weighting scheme can alleviate unnecessary views' adverse effects and enlarge the positive effects of the important views by assigning smaller and larger weights, respectively. In addition, we provide theoretical investigations about the convergence, perturbation analysis, and generalization error of the WM-NMF algorithm. Experimental results confirm the effectiveness and advantages of the proposed algorithm in terms of achieving better clustering performance and dealing with the corrupted data compared to the existing algorithms.

Keywords: Clustering, Data Integration, Multi-view Data, Nonnegative Matrix Factorization, Weighting

1. Introduction

Learning multi-view data is an emerging problem in machine learning research, as multi-view data becomes more and more common in many real-world applications. For example, the multi-omics data are now ubiquitous where different biological layers such as genomics, epigenomics, transcriptomics, and proteomics can be obtained from the same set of objects (Hasin et al., 2017; Lloyd-Price et al., 2019; Bhattacharya et al.,

2021). In those scenarios, the same set of objects has different views collected from different measuring methods or modalities, where any particular single-view data may be inadequate to comprehensively describe the information of all the objects. Hence, one major goal of multi-view learning is to search for a consensus clustering across views so that similar objects are grouped into the same cluster and dissimilar objects are separated into different clusters. In the literature, such a learning problem is called multi-view clustering (Bickel and Scheffer, 2004).

There are mainly two groups of approaches in the existing literature: generative (model-based) and discriminative (similarity-based and dimension reduction-based) (Rappoport and Shamir, 2018). For the generative approach, we typically use the mixture model and regression-based matrix factorization. The idea is to model each data view’s probabilistic distribution and obtain a common clustering result by either allowing all views to share the same priors or derived from a shared latent factors (Lashkari and Golland, 2008; Shen et al., 2009; Tzortzis and Likas, 2009, 2010; Savage et al., 2010; Lock and Dunson, 2013; Gabasova et al., 2017). An advantage of the generative approach is that it provides a nice interpretation of what the cluster is built on, but this approach is computationally more expensive in the context of multi-view learning. The discriminative approach focuses on the objective function that optimizes the average similarities within clusters and dissimilarities between clusters. Different objective functions result in different methods, such as multi-view spectral clustering methods (Wang et al., 2013; Kumar and Daumé, 2011; Kumar et al., 2011), nonnegative matrix factorization for multi-view learning (Liu et al., 2013; Kalayeh et al., 2014; Yang and Michailidis, 2015; Huang et al., 2014; Zhang et al., 2012), and canonical correlation analysis (Chaudhuri et al., 2009; Klami et al., 2013; Lai and Fyfe, 2000; Witten and Tibshirani, 2009; Chen et al., 2013).

Nonnegative matrix factorization (NMF) is a well-known algorithm for dimension reduction and feature extraction for nonnegative data. Unlike other matrix factorization techniques (Golub and Reinsch, 1970; Abdi and Williams, 2010; Zhao et al., 2015), NMF provides a more intuitive and interpretable understanding through the *parts-based representation*: a data point can be represented by only a few activated basis elements (Turk and Pentland, 1991; Lee and Seung, 1999). NMF has been shown the advantages of extracting sparse and meaningful information from high-dimensional data (Lee and Seung, 1999). The theoretical analysis further reveals the equivalence of NMF and spectral clustering and K-means clustering (Ding et al., 2005). Thus, NMF can also be viewed as a clustering method. The multi-view NMF (MultiNMF) (Liu et al., 2013) is an extension of NMF problem to integrate multiple nonnegative data matrices obtained from a common set of data points. The framework of MultiNMF attempts to approximate each view with some constraints in order to obtain both consensus and modality-specific information. Existing related methods tackle this problem with different objective functions motivated by different applications (Zhang et al., 2012; Li et al., 2012; Jin and Lee, 2015; Yang and Michailidis, 2015). However, most existing MultiNMF related methods either assume that

all views are equally important or the view-specific weights are known a priori in deriving the consensus clustering. In practice, such an assumption may not be valid as we often have noisy and corrupted datasets.

The aim of this paper is to design an effective multi-view NMF algorithm that not only can perform multi-view clustering but also quantify each view’s and each observation’s information content through learning both the view-specific and observation-specific view weights. We expect the new strategies to improve the clustering performance over traditional multi-view learning approaches.

Our major contributions include: (1) The proposed method extends and improves the existing MultiNMF method by automatically computing both the view-specific and observation-specific view weights without requiring the use of prior knowledge. The two types of weights provide two different resolutions in understanding the effect of different views. Thus, the consensus matrix can be obtained by weighting different views, which efficiently extracts different information qualities from each view. (2) We study the properties of these two weighting schemes and provide guidance on choosing the tuning parameter. (3) We develop theorems about the convergence, perturbation analysis, and generalization error of the proposed algorithm.

The rest of the paper is organized as follows. In Section 2, we introduce notations and overview existing techniques most relevant to our proposed methods. In Section 3 and 4, we present our proposed multi-view weighted NMF (WM-NMF) algorithm and study the optimization procedure. In Section 5, we provide theoretical analyses on the proposed method including algorithm convergence, perturbation analysis, and generalization error bound. In Section 6, experimental results are reported for both simulated and real data including handwritten digit data and multi-omics biological data. Comparisons are made with some competing models and popular methods. We conclude with discussions in Section 7.

2. Preliminary

Denote a nonnegative data matrix $\mathbf{X} = (\mathbf{x}_1, \dots, \mathbf{x}_N) \in \mathbb{R}_+^{M \times N}$, where $\mathbf{x}_i = (x_{1i}, \dots, x_{Mi})^\top \in \mathbb{R}_+^M$ is the i th data point of \mathbf{X} containing M features. NMF factorizes \mathbf{X} into a product of two lower-dimensional nonnegative matrices: $\mathbf{X} \approx \mathbf{U}\mathbf{V}^\top$, where $\mathbf{U} \in \mathbb{R}_+^{M \times K}$, $\mathbf{V} \in \mathbb{R}_+^{N \times K}$, and $K < \min(M, N)$ is a positive integer. We formulate the NMF problem as the following Frobenius norm optimization problem. The NMF problem is in general nonconvex and NP-hard, but it can be solved with iterative updates that work well in many applications (Lee and Seung, 1999, 2001):

$$\min_{\mathbf{U}, \mathbf{V} \geq 0} \left\| \mathbf{X} - \mathbf{U}\mathbf{V}^\top \right\|_F^2; \quad \mathbf{U}_{j,k} \leftarrow \mathbf{U}_{j,k} \frac{(\mathbf{X}\mathbf{V})_{j,k}}{(\mathbf{U}\mathbf{V}^\top \mathbf{V})_{j,k}}, \quad \mathbf{V}_{i,k} \leftarrow \mathbf{V}_{i,k} \frac{(\mathbf{X}^\top \mathbf{U})_{i,k}}{(\mathbf{V}\mathbf{U}^\top \mathbf{U})_{i,k}},$$

where $\|\cdot\|_F$ denotes the Frobenius norm. \mathbf{U} is the basis matrix that each column is a basis element, which serves as the building block for reconstruction to the original data point. \mathbf{V} is the coefficient matrix that each row provides the coordinates of each

data point in \mathbf{U} . Thus, each data point is approximated by a linear combination of the building blocks with weights given by each row of \mathbf{V} . Different from other matrix factorization techniques, NMF provides a more intuitive and interpretable understanding through the *parts-based representation*: a data point can be represented by only a few activated basis elements. Further, \mathbf{V} directly translates to data clustering by simply assigning each data point to the basis element on which it has the highest loading; that is, data point i is placed in cluster j if $\mathbf{V}_{i,j}$ is the largest entry in row i . Ding et al. (2005) further shows the equivalence between NMF and K -means and spectral clustering.

The multi-view NMF (MultiNMF) (Liu et al., 2013) is an extension of NMF problem to integrate multiple nonnegative data matrices obtained from a common set of data points and conducts clustering based on the low-rank representations. Let $\{\mathbf{X}^{(1)}, \dots, \mathbf{X}^{(n_v)}\}$ be a set of n_v views of data points, with $\mathbf{X}^{(s)} \in \mathbb{R}_+^{M_s \times N}$. Without loss of generality, we assume all the data matrices are pre-processed and transformed when necessary. The framework of MultiNMF attempts to approximate each view $\mathbf{X}^{(s)} \approx \mathbf{U}^{(s)}\mathbf{V}^{(s)\top}$ with some constraints in order to obtain both consensus and view-specific information. More specifically, the MultiNMF solves the following optimization problem:

$$\min_{\mathbf{U}^{(s)}, \mathbf{V}^{(s)}, \mathbf{V}^* \geq 0} \sum_{s=1}^{n_v} \left\| \mathbf{X}^{(s)} - \mathbf{U}^{(s)}\mathbf{V}^{(s)\top} \right\|_F^2 + \sum_{s=1}^{n_v} \alpha_s \left\| \mathbf{V}^{(s)}\mathbf{Q}^{(s)} - \mathbf{V}^* \right\|_F^2. \quad (1)$$

The first part of the objective function performs NMF analysis independently on each view. The second part plays a key role in sharing information across views, and it regularizes the learned coefficient matrices $\mathbf{V}^{(s)}$'s towards a common \mathbf{V}^* . We take \mathbf{V}^* as some latent data structure shared by all views. The amount of information for each view contributing to \mathbf{V}^* is regularized by α_s . Thus, α_s is the parameter that tunes the relative weight among views. $\mathbf{Q}^{(s)} = \text{Diag}(\sum_{j=1}^{M_s} u_{j1}^{(s)}, \sum_{j=1}^{M_s} u_{j2}^{(s)}, \dots, \sum_{j=1}^{M_s} u_{jK}^{(s)})$, where $\text{Diag}(\cdot)$ denotes a diagonal matrix with diagonal elements equal to the values in the parenthesis sequentially. $\mathbf{Q}^{(s)}$ constrains the column sums of $\mathbf{U}^{(s)}$ so that $\mathbf{V}^{(s)}$'s are comparable across views. The above optimization problem can be solved by an iterative update procedure.

In the MultiNMF framework, α_s 's are crucial in determining the quality of the consensus matrix \mathbf{V}^* . To illustrate this point, on one hand, if there is a disagreement between the s -th view and the others, i.e., the s -th view provides contrasting subspace structure compared with other views, α_s should approach to 0. On the other hand, if all views provide similar information on subspace structure, α_s 's should be close to each other. The MultiNMF degenerates to the single-view learning when α_s 's are binary values with only one component being 1. The resulting consensus clustering is essentially determined by the view that provides the best approximation to the original data.

Most existing MultiNMF related methods tackle different problems with slightly different objective functions motivated by different applications (Zhang et al., 2012;

Li et al., 2012; Jin and Lee, 2015; Yang and Michailidis, 2015). However, most of them assume that the weight vector is determined either by prior knowledge (which may be impractical when such knowledge is missing) or commonly assigned as equal weight. In practice, such an assumption may not be valid as we often have noisy and corrupted datasets. In Section 3, we provide an alternative solution to allow a more interpretable and transparent understanding of how to derive the consensus clustering among views.

3. Weighted multi-view NMF

To take the advantage of the consensus matrix used in MultiNMF and learn the weight vector automatically, we adopt the idea of exponential parameter to automatically quantify each view’s information content (Tzortzis and Likas, 2009; Xu et al., 2016). In addition, as demonstrated in the handwritten digit dataset and the multi-omics data for liver hepatocellular carcinoma from Section 6, data points in one sample are likely heterogeneous that contain clusters determined by different views. Thus, it is also important to determine the weights describing each view’s relative information content for each observation. We refer to such weight as observation-specific view weight. In this paper, we propose a weighted multi-view NMF (WM-NMF) framework for a more interpretable data integration procedure, while it achieves the ability to automatically update both view and observation-specific weights. More specifically, WM-NMF works on minimizing the following objective function:

$$\mathcal{O} = \sum_{s=1}^{n_v} \left\| \left\{ \mathbf{X}^{(s)} - \mathbf{U}^{(s)} \mathbf{V}^{(s)\top} \right\} \text{Diag}(\mathbf{w}^{(s)}) \right\|_F^2 + \sum_{s=1}^{n_v} \alpha_s^p \left\| \mathbf{V}^{(s)} \mathbf{Q}^{(s)} - \mathbf{V}^* \right\|_F^2 + \beta g(\mathbf{V}^{(1:n_v)}), \quad (2)$$

where $\mathbf{w}^{(s)} = (w_1^{(s)}, \dots, w_N^{(s)})^\top$. $w_i^{(s)}$ is the weight for view s and data point i . $g(\mathbf{V}^{(1:n_v)})$ is a regularization term on $\mathbf{V}^{(1)}, \dots, \mathbf{V}^{(n_v)}$ which can be set for different purposes, such as sparse NMF (Hoyer, 2004), orthogonal NMF (Zhang et al., 2019; Liang et al., 2020), and graph NMF (Cai et al., 2010; Huang et al., 2014). $\beta > 0$ is the corresponding tuning parameter. We minimize \mathcal{O} over $\mathbf{U}^{(s)}, \mathbf{V}^{(s)}, \mathbf{w}^{(s)}, \alpha_s, s = 1, \dots, n_v$, and \mathbf{V}^* under the constraints that $\mathbf{V}^* \geq 0, \mathbf{V}^{(s)} \geq 0, \mathbf{U}^{(s)} \geq 0, \sum_{s=1}^{n_v} \alpha_s = 1, \alpha_s \geq 0, \sum_{s=1}^{n_v} w_i^{(s)} = 1, w_i^{(s)} \geq 0, s = 1 : n_v, i = 1 : N$.

Here, $p \geq 1$ is the exponential parameter and it controls the sparsity of α_s . The vector $\boldsymbol{\alpha} = (\alpha_1, \dots, \alpha_{n_v})^\top$ represents the relative weight among different views and the agreement between $\mathbf{V}^{(s)}$ and \mathbf{V}^* . It reflects each view’s contribution for reaching the consensus matrix \mathbf{V}^* . $w_i^{(s)}$ is the weight for view s and i th observation. Its functionality is different from the view-specific weights, where α_s provides an overall measure to quantify the contribution from view s towards a consensus matrix. Intuitively, a smaller value of $w_i^{(s)}$ implies that the s -th view fails to provide a good approximation to observation i . The introduction of $w_i^{(s)}$ provides the flexibility to allow one view

to compensate for the shortcoming in another, and potentially prevents the spurious results from outliers or highly divergent views. More specifically, by constraining $\sum_{s=1}^{n_v} w_i^{(s)} = 1$ and $\sum_{s=1}^{n_v} \alpha_s = 1$, it ensures the feasibility to automatically update the weights as demonstrated in Section 4.

WM-NMF framework extends and improves the existing literature with several benefits. First, it automatically computes the weight vectors without relying on any prior knowledge. Second, it calculates the consensus matrix by weighting different coefficient matrices, which efficiently extracts different qualities of information from each view. Third, it can alleviate the negative effects of unimportant views and enlarge the positive effects of important views by assigning small and large weights on different views and observations, respectively. Lastly, additional regularization can be easily incorporated based on our WM-NMF framework. For example, a manifold regularization can be used to further improve the clustering results (Cai et al., 2010).

The idea of manifold regularization is based on the local invariance assumption such that the geometric structure of the original dataset is inherited in the low-rank representations (Belkin and Niyogi, 2001). To extend the existing manifold regularization for single-view NMF to accommodate our multi-view NMF, we first define an adjacency matrix $\mathbf{A}^{(s)}$ to measure the closeness between any two data points represented by view s . Using the Gaussian kernel, it is defined as

$$a_{ij}^{(s)} = \begin{cases} \exp\left(-\frac{\|\mathbf{x}_i^{(s)} - \mathbf{x}_j^{(s)}\|_2^2}{\sigma^2}\right), & \text{if } \mathbf{x}_j^{(s)} \in \mathcal{N}_i^{(s)}; \\ 0, & \text{otherwise;} \end{cases}$$

where $\mathcal{N}_i^{(s)}$ denotes the neighbour for point i represented by view s . $\mathcal{N}_i^{(s)}$ is generated using K -nearest neighbour which utilizes the distance between two data points: $\|\mathbf{x}_i^{(s)} - \mathbf{x}_j^{(s)}\|_2^2$. The number of neighbours is set to be 5 and $\sigma^2 = 1$ as suggested in Cai et al. (2010).

Thus, together with the corresponding low-dimensional representation $\mathbf{v}_i^{(s)}$, the manifold regularization is defined as

$$S = \frac{1}{2} \sum_{i,j=1}^N \left\| \mathbf{v}_i^{(s)} - \mathbf{v}_j^{(s)} \right\|^2 a_{ij}^{(s)} = \text{Tr} \left(\mathbf{V}^{(s)\top} \mathbf{L}^{(s)} \mathbf{V}^{(s)} \right),$$

where $\mathbf{L}^{(s)} = \mathbf{D}^{(s)} - \mathbf{A}^{(s)}$ is the graph Laplacian matrix and \mathbf{D} is a diagonal matrix with the i th diagonal entry being $\sum_{j=1}^N a_{ij}^{(s)}$. $\text{Tr}(\cdot)$ denotes the trace of a matrix. By minimizing S , we expect that if $\mathbf{x}_i^{(s)}$ and $\mathbf{x}_j^{(s)}$ are close, i.e., $a_{ij}^{(s)}$ is large, the corresponding low-dimensional representations $\mathbf{v}_i^{(s)}$ and $\mathbf{v}_j^{(s)}$ are also close together.

Replacing $g(\mathbf{V}^{(1:n_v)})$ in Eq. (2) by the above manifold regularization, we can define the objective function of the manifold regularized WM-NMF as

$$\begin{aligned} \mathcal{O} = & \sum_{s=1}^{n_v} \left\| \left\{ \mathbf{X}^{(s)} - \mathbf{U}^{(s)} \mathbf{V}^{(s)\top} \right\} \text{Diag}(\mathbf{w}^{(s)}) \right\|_F^2 + \sum_{s=1}^{n_v} \alpha_s^p \left\| \mathbf{V}^{(s)} \mathbf{Q}^{(s)} - \mathbf{V}^* \right\|_F^2 + \\ & \beta \sum_{s=1}^{n_v} \text{Tr}(\mathbf{V}^{(s)\top} \mathbf{L}^{(s)} \mathbf{V}^{(s)}), \end{aligned} \quad (3)$$

We will discuss how to choose β in the experiment section. The scenario for WM-NMF without manifold regularization can be retrieved by setting $\beta = 0$. An illustration of the manifold regularized WM-NMF is shown in Figure 1. In Section 4, all the results are based on the objective function \mathcal{O} in Eq. (3).

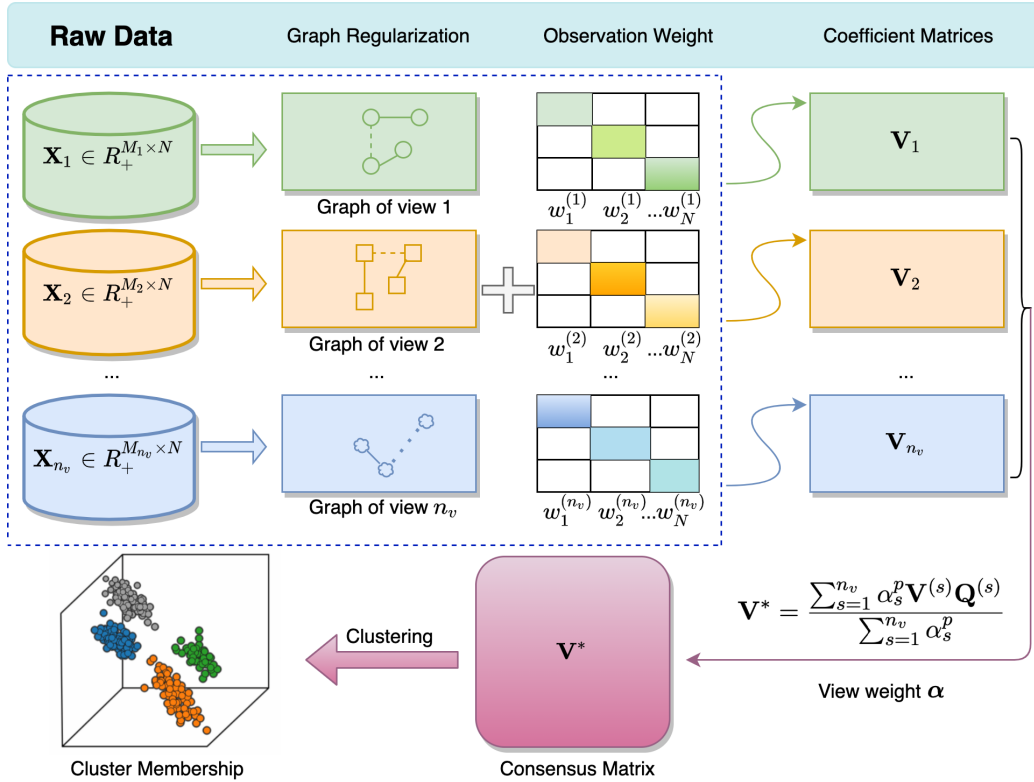


Figure 1: The illustration of the weighted multi-view NMF with manifold regularization for clustering.

4. Optimization

The joint optimization function in Eq. (3) is nonconvex over all variables. However, if we keep four of the five variables ($\mathbf{U}^{(s)}$, $\mathbf{V}^{(s)}$, \mathbf{V}^* , α , $\mathbf{w}^{(s)}$) fixed, and we optimize over

one of them, the problem is convex and can be solved efficiently. We thus consider the following iterative alternating minimization method that until convergence, at each iteration, we optimize over the five variables alternatively.

More specifically, we first update $\mathbf{U}^{(s)}$ and $\mathbf{V}^{(s)}$ individually while keeping the others fixed. We call these procedures the *inner iteration* because updating $\mathbf{U}^{(s)}$ or $\mathbf{V}^{(s)}$ only needs to solve the single-view objective function represented by

$$\mathcal{O}_0 = \left\| \left\{ \mathbf{X}^{(s)} - \mathbf{U}^{(s)} \mathbf{V}^{(s)\top} \right\} \text{Diag}(\mathbf{w}^{(s)}) \right\|_F^2 + \alpha_s^p \left\| \mathbf{V}^{(s)} \mathbf{Q}^{(s)} - \mathbf{V}^* \right\|_F^2 + \beta \text{tr} \left(\mathbf{V}^{(s)\top} \mathbf{L}^{(s)} \mathbf{V}^{(s)} \right). \quad (4)$$

After obtaining $\mathbf{U}^{(s)}$ and $\mathbf{V}^{(s)}$, we solve the exact solutions of $\boldsymbol{\alpha}$, $\mathbf{w}^{(s)}$ and \mathbf{V}^* . We call these procedures the *outer iteration*.

4.1 Update $\mathbf{U}^{(s)}$

To simplify the notation, we omit the view index (s) for the derivations of the inner iteration. Minimizing the objective function \mathcal{O} for \mathbf{U} is equivalent to minimizing the objective function

$$\begin{aligned} \mathcal{O}_1 &= \left\| \left\{ \mathbf{X} - \mathbf{U} \mathbf{V}^\top \right\} \text{Diag}(\mathbf{w}) \right\|_F^2 + \alpha_s^p \left\| \mathbf{V} \mathbf{Q} - \mathbf{V}^* \right\|_F^2 \\ &= \text{tr} \left[(\mathbf{X} - \mathbf{U} \mathbf{V}^\top) \text{Diag}^2(\mathbf{w}) (\mathbf{X}^\top - \mathbf{V} \mathbf{U}^\top) \right] + \alpha_s^p \text{tr} (\mathbf{V} \mathbf{Q} \mathbf{Q}^\top \mathbf{V}^\top - 2 \mathbf{V} \mathbf{Q} \mathbf{V}^{*\top} + \mathbf{V}^* \mathbf{V}^{*\top}). \end{aligned}$$

Taking the derivative of \mathcal{O}_1 with respect to u_{ij} while taking into account of the nonnegative constraint on u_{ik} , and using the complementary slackness condition $\Psi_{ik} u_{ik} = 0$, where Ψ_{ik} is the Lagrange multiplier for the constraint $u_{ik} \geq 0$ leads to the multiplicative update rule of u_{ik} :

$$\begin{aligned} u_{ik} &\leftarrow u_{ik} \frac{[\mathbf{X} \text{Diag}^2(\mathbf{w}) \mathbf{V}]_{ik} + \alpha_s^p \sum_{j=1}^N v_{jk} v_{jk}^*}{[\mathbf{U} \mathbf{V}^\top \text{Diag}^2(\mathbf{w}) \mathbf{V}]_{ik} + \alpha_s^p \sum_{l=1}^M u_{lk} \sum_{j=1}^N v_{jk}^2} \\ &= u_{ik} - \underbrace{\frac{u_{ik}}{[\mathbf{U} \mathbf{V}^\top \text{Diag}^2(\mathbf{w}) \mathbf{V}]_{ik} + \alpha_s^p \sum_{l=1}^M u_{lk} \sum_{j=1}^N v_{jk}^2}}_{\text{step size}} \times \frac{1}{2} \nabla_U \mathcal{O}_1, \end{aligned} \quad (5)$$

where $\nabla_U \mathcal{O}_1 = \frac{\partial \mathcal{O}_1}{\partial u_{ik}}$. Details for the derivation is in Appendix A. The update is a gradient descent algorithm, where the step size should be nonzero. Therefore, we should initialize a positive u_{ik} , otherwise u_{ik} equals to 0 for all subsequent iterations. In addition, the following Theorem 1 ensures that u_{ik} will always be positive number and it will not get shrunk to 0.

4.2 Update $\mathbf{V}^{(s)}$

Similarly, we omit the view index (s) for notation simplicity. Again, minimizing the objective function \mathcal{O} with respect to \mathbf{V} is equivalent to minimizing the following

objective function denoted as \mathcal{O}_2 ,

$$\begin{aligned}\mathcal{O}_2 &= \left\| \{\mathbf{X} - \mathbf{U}\mathbf{V}^\top\} \text{Diag}(\mathbf{w}) \right\|_F^2 + \alpha_s^p \left\| \mathbf{V}\mathbf{Q} - \mathbf{V}^* \right\|_F^2 + \beta \text{tr}(\mathbf{V}^\top \mathbf{L} \mathbf{V}) \\ &= \text{tr} [(\mathbf{X}^\top - \mathbf{V}\mathbf{U}^\top) \text{Diag}^2(\mathbf{w})(\mathbf{X} - \mathbf{U}\mathbf{V}^\top)] + \alpha_s^p \mathbf{R} + \beta \text{tr} \mathbf{V}^\top \mathbf{L} \mathbf{V},\end{aligned}$$

where $\mathbf{R} = \text{tr} [(\mathbf{V}\mathbf{Q} - \mathbf{V}^*)(\mathbf{Q}^\top \mathbf{V}^\top - \mathbf{V}^{*\top})]$. Let Φ_{jk} be the Lagrange multiplier for the constraint $v_{jk} \geq 0$. Setting the derivative of \mathcal{O}_2 with respect to v_{jk} to be 0 while taking into consideration of the nonnegative constraint of v_{jk} , and using the complementary slackness condition $\Phi_{jk}v_{jk} = 0$, we have the multiplicative update rule of v_{jk} :

$$\begin{aligned}v_{jk} &\leftarrow v_{jk} \frac{[\text{Diag}^2(\mathbf{w})\mathbf{X}^\top \mathbf{U}]_{jk} + \alpha_s^p [\mathbf{V}^* \mathbf{Q}^\top]_{jk} + \beta [\mathbf{A}\mathbf{V}]_{jk}}{[\text{Diag}^2(\mathbf{w})\mathbf{V}\mathbf{U}^\top \mathbf{U}]_{jk} + \alpha_s^p [\mathbf{V}\mathbf{Q}\mathbf{Q}^\top]_{jk} + \beta [\mathbf{D}\mathbf{V}]_{jk}} \\ &= v_{jk} - \underbrace{\frac{v_{jk}}{[\text{Diag}^2(\mathbf{w})\mathbf{V}\mathbf{U}^\top \mathbf{U}]_{jk} + \alpha_s^p [\mathbf{V}\mathbf{Q}\mathbf{Q}^\top]_{jk} + \beta [\mathbf{D}\mathbf{V}]_{jk}}}_{\text{step size}} \times \nabla_V \mathcal{O}_2,\end{aligned}\quad (6)$$

where $\nabla_V \mathcal{O}_2 = \frac{\partial \mathcal{O}_2}{\partial v_{jk}}$, and $\mathbf{L} = \mathbf{D} - \mathbf{A}$ is the graph Laplacian matrix defined in Section 3. The update is a gradient descent algorithm, where the step size should be nonzero. Again, we should make sure the initialization of v_{jk} is positive, otherwise $v_{jk} = 0$ at all subsequent iterations.

Theorem 1 ensures that when we initialize positive u_{ik} and v_{jk} , the entries of \mathbf{U} and \mathbf{V} will always be updated as positive numbers, and the updated values will not get shrunk to 0.

Theorem 1 *If $u_{ik}^1 > 0$ and $v_{jk}^1 > 0$, $\forall i, j, k$, then $u_{ik}^t > 0$, $v_{jk}^t > 0$, $\forall i, j, k, \forall t \geq 1$, where t denotes the t -th update.*

Proof The proof is given in Appendix B. ■

4.3 Estimate α_s

This is equivalent to minimizing the following objective over α_s that

$$\min_{\alpha_s} \alpha_s^p \left\| \mathbf{V}^{(s)} \mathbf{Q}^{(s)} - \mathbf{V}^* \right\|_F^2, \text{ subject to } \sum_{s=1}^{n_v} \alpha_s = 1.$$

When $p = 1$, the optimal solution of α_s is

$$\hat{\alpha}_s = \begin{cases} 1, & s = \arg \min_{s' \in 1, \dots, n_v} \left\| \mathbf{V}^{(s')} \mathbf{Q}^{(s')} - \mathbf{V}^* \right\|_F^2 \\ 0, & \text{otherwise.} \end{cases}$$

The above solution implies that $p = 1$ only offers a binary solution of α_s , i.e., the consensus matrix \mathbf{V}^* depends on a single view. Such a solution is obviously too restrictive, as it prevents the partial information sharing among views. On the other hand, when $p > 1$, we obtain the optimal solution for $\boldsymbol{\alpha}$ as:

$$\hat{\alpha}_s = \frac{1}{\sum_{s'=1}^{n_v} \left(\frac{\|\mathbf{V}^{(s)}\mathbf{Q}^{(s)} - \mathbf{V}^*\|_F^2}{\|\mathbf{V}^{(s')}\mathbf{Q}^{(s')} - \mathbf{V}^*\|_F^2} \right)^{\frac{1}{p-1}}}. \quad (7)$$

The solution implies that when the s -th view's information content contributes more to the consensus matrix, i.e., $\|\mathbf{V}^{(s)}\mathbf{Q}^{(s)} - \mathbf{V}^*\|_F^2$ is smaller, $\hat{\alpha}_s$ becomes larger. Therefore, the more important the view is, the larger the corresponding weight is.

Theorem 2 *The exponential parameter p controls the sparsity of the weight vector through Eq. (7).*

Proof Denote $A^{(s)} = \|\mathbf{V}^{(s)}\mathbf{Q}^{(s)} - \mathbf{V}^*\|_F^2$ and $A^{(s')} = \|\mathbf{V}^{(s')}\mathbf{Q}^{(s')} - \mathbf{V}^*\|_F^2$. It is clear that as p goes to infinity, the denominator of Eq. (7) converges to n_v , which gives uniform weights to each view. Meanwhile, if the normalized s -th view $\mathbf{V}^{(s)}\mathbf{Q}^{(s)}$ contributes the most to the consensus matrix \mathbf{V}^* , i.e., $A^{(s)}/A^{(s')} < 1$ for $s' \neq s$, then $p \rightarrow 1^+$ implies $\alpha_s \rightarrow 1$. On the other hand, if the normalized s -th view $\mathbf{V}^{(s)}\mathbf{Q}^{(s)}$ contributes the least to the consensus matrix \mathbf{V}^* , i.e., $A^{(s)}/A^{(s')} > 1$ for $s' \neq s$, then $p \rightarrow 1^+$ implies $\alpha_s \rightarrow 0$. Hence, a smaller p results in a sparser weight vector $\boldsymbol{\alpha}$. ■

As mentioned in Section 3, a moderate size p should be used so that the relevant information from different views is preserved and the effect of consensus constraint is kept.

4.4 Estimate $w_i^{(s)}$

To optimize $w_i^{(s)}$, we only consider the terms involving $w_i^{(s)}$ in the objective that we consider

$$\begin{aligned} & \min_{\mathbf{w}^{(s)} \geq 0, \sum_{s=1}^{n_v} w_i^{(s)} = 1} \left\| \left\{ \mathbf{X}^{(s)} - \mathbf{U}^{(s)}\mathbf{V}^{(s)\top} \right\} \text{Diag}(\mathbf{w}^{(s)}) \right\|_F^2 \\ &= \text{tr} \left[\text{Diag}(\mathbf{w}^{(s)}) (\mathbf{X}^{(s)\top} - \mathbf{V}^{(s)}\mathbf{U}^{(s)\top}) (\mathbf{X}^{(s)} - \mathbf{U}^{(s)}\mathbf{V}^{(s)\top}) \text{Diag}(\mathbf{w}^{(s)}) \right] \\ &= \sum_{i=1}^N w_i^{(s)2} \sum_{j=1}^{M_s} \mathbf{Y}_{ji}^{(s)2}, \end{aligned}$$

where $\mathbf{Y}^{(s)} = \mathbf{X}^{(s)} - \mathbf{U}^{(s)}\mathbf{V}^{(s)\top}$. Since we only optimize the weight for a single observation, it is equivalent to minimizing $w_i^{(s)2} \sum_{j=1}^{M_s} \mathbf{Y}_{ji}^{(s)2}$ with the constraints that $\sum_{s=1}^{n_v} w_i^{(s)} = 1$ and $w_i^{(s)} \geq 0$. We have that the optimal solution is

$$\hat{w}_i^{(s)} = \left(\sum_{s'=1}^{n_v} \frac{1}{\sum_{j=1}^{M_{s'}} (\mathbf{Y}_{ji}^{(s')})^2} \sum_{j=1}^{M_s} (\mathbf{Y}_{ji}^{(s)})^2 \right)^{-1}. \quad (8)$$

The above solution shows that the observation-specific view weight is determined by the approximation error of the s -th modality on the i -th object across all the features. The smaller the error is compared with other views, the larger the weight is.

4.5 Estimate \mathbf{V}^*

To optimize \mathbf{V}^* , we only consider the terms involving \mathbf{V}^* in the objective \mathcal{O} :

$$\mathcal{O}_v = \sum_{s=1}^{n_v} \alpha_s^p \left\| \mathbf{V}^{(s)} \mathbf{Q}^{(s)} - \mathbf{V}^* \right\|_F^2 = \sum_{s=1}^{n_v} \alpha_s^p \text{tr} \left(\mathbf{V}^{(s)} \mathbf{Q}^{(s)} \mathbf{Q}^{(s)\top} \mathbf{V}^{(s)\top} - 2 \mathbf{V}^{(s)} \mathbf{Q}^{(s)} \mathbf{V}^{*\top} + \mathbf{V}^* \mathbf{V}^{*\top} \right).$$

Setting the derivative of \mathcal{O}_v with respect to \mathbf{V}^* to 0, we have that the optimal solution is

$$\mathbf{V}^* = \frac{\sum_{s=1}^{n_v} \alpha_s^p \mathbf{V}^{(s)} \mathbf{Q}^{(s)}}{\sum_{s=1}^{n_v} \alpha_s^p}. \quad (9)$$

Since $\mathbf{V}^{(s)} \geq 0$, $\mathbf{Q}^{(s)} \geq 0$, and $\alpha_s > 0$, \mathbf{V}^* is nonnegative. The underlying assumption of the multi-view clustering is that all the views can agree and reduce to a consensus matrix with different weights, so the cluster assignments can be determined according to the consensus matrix \mathbf{V}^* . The connection between NMF and probabilistic latent semantic analysis (PLSA) suggests that the cluster assignment for observation i is determined by the largest entry in row i of \mathbf{V}^* (Gaussier and Goutte, 2005). However, Welch et al. (2019) points out the spurious alignments in highly divergent datasets by the maximum coefficient assignments. In the experiment section, we use the default `spectralcluster` in MATLAB on \mathbf{V}^* to obtain the cluster membership.

4.6 Summary of the algorithm

We summarize the pseudocode of the WM-NMF algorithm below. The algorithm stops when the maximum number of iterations is reached or it converges, i.e., when the difference between the two consecutive iterations is less than the threshold 9×10^{-8} . The algorithm converges to the local minima since the objective function is nonconvex.

4.7 Choice of K

A larger value of K better approximates the original data, but on the other hand, it raises the risk of overfitting. Many approaches have been developed to select the number of basis elements K for the NMF problem. For example, Owen et al. (2009) proposes the Bi-cross validation method which partitions \mathbf{V} into a few parts and predicts the withheld part based on the other observed parts. The optimal K is chosen when the prediction error is minimized. Ulfarsson and Solo (2013) proposes to choose K when the Stein’s unbiased risk estimator of mean squared error is minimized. Nevertheless, the variance of the model error is another parameter and how to choose or estimate it poses another problem. Moreover, Squires et al. (2017) argues the above

Algorithm 1: Weighted Multi-View NMF (WM-NMF)

Input : Dataset $\{\mathbf{X}^{(1)}, \dots, \mathbf{X}^{(n_v)}\}$; rank K ; exponential parameter p ;
manifold parameter β .
Output: Basis matrices $\mathbf{U}^{(1)}, \dots, \mathbf{U}^{(n_v)}$; Coefficient matrices $\mathbf{V}^{(1)}, \dots, \mathbf{V}^{(n_v)}$;
Consensus matrix \mathbf{V}^* ; View weight vector α_s for each view;
Observation weight w_i for each view.

- 1 Normalize each view $\mathbf{X}^{(s)}$ such that $\|\mathbf{X}^{(s)}\|_1 = 1$.
- 2 Initialize $\mathbf{U}^{(s)}, \mathbf{V}^{(s)}, \mathbf{V}^*$ for $s = 1, \dots, n_v$, set equal view weight $\alpha_s = 1/n_v$
and observation weight $w_i^{(s)} = 1/N$.
- 3 **repeat** \leftarrow (outer iteration)
- 4 **for** $s = 1 : n_v$ **do** \leftarrow (inner iteration)
- 5 **repeat**
- 6 Fixing $\mathbf{w}^{(s)}, \alpha, \mathbf{V}^*$ and $\mathbf{V}^{(s)}$, update $\mathbf{U}^{(s)}$ by Eq. (5);
- 7 Fixing $\mathbf{w}^{(s)}, \alpha, \mathbf{V}^*$ and $\mathbf{U}^{(s)}$, update $\mathbf{V}^{(s)}$ by Eq. (6);
- 8 **until** \mathcal{O}_0 converges or the maximum number of iteration is reached.
- 9 **end for**
- 10 Fixing $\mathbf{w}^{(s)}, \mathbf{U}^{(s)}, \mathbf{V}^{(s)}$, $s = 1, \dots, n_v$, and \mathbf{V}^* , update α by Eq. (7);
- 11 Fixing $\alpha, \mathbf{U}^{(s)}, \mathbf{V}^{(s)}$, and \mathbf{V}^* , update \mathbf{w} by Eq. (8);
- 12 Fixing $\mathbf{w}^{(s)}, \mathbf{U}^{(s)}, \mathbf{V}^{(s)}$, $s = 1, \dots, n_v$, and α , update \mathbf{V}^* by Eq. (9);
- 13 **until** the maximum number of iteration is reached or the algorithm
converges.
- 14 Perform clustering analysis based on \mathbf{V}^* .

error-based methods are not ideal as good results can be achieved by fine tuning the parameters. Instead, it proposes to use the minimum description length (MDL) method which takes into account of both model error and model complexity. A small rank implies few parameters to estimate and thus reduces the model complexity, but increases the model error. While a large rank has a reverse effect. Thus, the rank is chosen when the summation of model complexity and model error is minimized. However, this method depends on the data precision, which is another tuning parameter that needs to be specified. Furthermore, Lin and Boutros (2020) proposes a missing value imputation method for the rank selection. More specifically, some entries of the data is randomly selected to be missing, and NMF is used to impute the missing values. It removes the rows in \mathbf{V} if these rows have missingness in \mathbf{X} when updating the rows of \mathbf{U} . Thus, the rank is chosen when the distance between the original entries and recovered entries is minimized.

Overall, all these methods show the capacity of selecting K empirically, and they can be easily extended to the multi-view NMF problem. In Section 6, we show that WM-NMF works considerably well within a range of K in terms of the clustering accuracy. Thus, it is quite robust to the choice of K .

4.8 Algorithm complexity analysis

We analyze the complexity for updating $\mathbf{U}^{(s)}$ and $\mathbf{V}^{(s)}$ in the inner iteration. We divide the counts of iterations into multiplication, addition and division. The overall complexity for the inner iteration is $O(M_s NK + N^2 K)$ (we provide the details in appendix A). We summarize the operation counts in Table 1.

Table 1: Computational operation counts for each iteration of $\mathbf{U}^{(s)}$ and $\mathbf{V}^{(s)}$.

| | multiplication | addition | division | overall |
|--------------------|--|---|----------|----------------------|
| $\mathbf{U}^{(s)}$ | $N + M_s N + M_s N K + (N + 1)K + N + K N + 2M_s N K + K(N + 2)$ | $K M_s N + N K + 2M_s N K + K(M_s + N)$ | $M_s K$ | $O(M_s N K)$ |
| $\mathbf{V}^{(s)}$ | $N + M_s N + M_s N K + 2N K + N^2 K + N + K N + 2M_s N K + 3K N + K$ | $K M_s N + N^2 K + 2M_s N K + K N^2$ | $N K$ | $O(M_s N K + N^2 K)$ |

Further, suppose there are t_1 iterations for updating $\mathbf{U}^{(s)}$ and $\mathbf{V}^{(s)}$ for each view, then the complexity for all views is $O\{t_1 n_v (M_* N K + N^2 K)\}$, where M_* denotes the maximum of $\{M_1, \dots, M_{n_v}\}$. After the t_1 inner iterations of $\mathbf{U}^{(s)}$ and $\mathbf{V}^{(s)}$, we still need $O(n_v)$ for α_s , $O(n_v N K)$ for \mathbf{V}^* , and $O(n_v N)$ for $\text{Diag}(\mathbf{w})$. Therefore, for each iteration of the whole procedure of Algorithm 1 (lines 4-12), the total complexity is $O\{t_1 n_v (M_* N K + N^2 K)\}$. Suppose t_2 outer iterations are taken for \mathcal{O} to converge or reaching the maximum number of iteration, then the overall algorithm takes time $O\{t_1 t_2 n_v (M_* N K + N^2 K)\}$ for $N > M_*$. When $N < M_*$, we have the overall complexity $O\{t_1 t_2 n_v M_* N K\}$.

5. Theoretical analysis

In this section, we analyze the proposed algorithm theoretically. First, we prove that the algorithm is nonincreasing. Second, we show that the local solution can be seen as an additive noise to the unique solution. Third, we analyze the generalization error bound of WM-NMF.

5.1 Convergence of the algorithm

First, we define the auxiliary function, which is widely used in the proof of convergence in the multiplicative update rules.

Definition 3 *A function $G(h, h')$ is called an auxiliary function of the function $J(h)$ if $G(h, h') \geq J(h)$ and $G(h, h) = J(h)$ for any h and h' .*

Lemma 4 (Lee and Seung (2001)) *If $G(h, h')$ is an auxiliary function of $J(h)$, then $J(h)$ is nonincreasing under the update rule*

$$h^{(t+1)} = \underset{h}{\operatorname{argmin}} G(h, h^{(t)}). \quad (10)$$

This is true because $J(h^{(t+1)}) \leq G(h^{(t+1)}, h^{(t)}) \leq G(h^{(t)}, h^{(t)}) = J(h^{(t)})$.

Theorem 5 *The objective function \mathcal{O} is nonincreasing under Algorithm 1.*

The proof is given in Appendix B. We verify Theorem 5 through different datasets in Section 6.

5.2 Perturbation analysis

As mentioned before, the WM-NMF algorithm finds the local solution only. It is a challenge to find the unique solution without certain regularizations (Laurberg et al., 2008; Gillis, 2012) and therefore the exact estimation error. However, the nonuniqueness can be formulated as estimation noise shown in Corollary 7, so we can bound the estimation error with a certain noise level in a similar way to Laurberg et al. (2008).

Theorem 6 *Let $(\mathbf{U}^{(s)}, \mathbf{V}^{(s)})$ be the unique solution of $\mathbf{X}^{(s)}$ (i.e., $\mathbf{X}^{(s)} = \mathbf{U}^{(s)}\mathbf{V}^{(s)\top}$) by minimizing \mathcal{O} defined in Eq. (3). Given some $\epsilon > 0$, there exists a $\delta > 0$ such that any nonnegative matrix $\mathbf{Y}^{(s)} = \mathbf{X}^{(s)} + \mathbf{E}^{(s)}$, where $\|\mathbf{E}^{(s)}\|_F < \delta$, satisfies*

$$D_{(\mathbf{U}^{(s)}, \mathbf{V}^{(s)})}(\mathbf{U}'^{(s)}, \mathbf{V}'^{(s)}) = \left(\|\mathbf{U}^{(s)} - \mathbf{U}'^{(s)}\|_F + \|\mathbf{V}^{(s)} - \mathbf{V}'^{(s)}\|_F \right) < \epsilon,$$

where D is a distance that measures the closeness between the unique solution $(\mathbf{U}^{(s)}, \mathbf{V}^{(s)})$ and the estimated $(\mathbf{U}'^{(s)}, \mathbf{V}'^{(s)})$. $(\mathbf{U}'^{(s)}, \mathbf{V}'^{(s)})$ is the local solution of $\mathbf{Y}^{(s)}$ estimated by the WM-NMF algorithm.

We provide the proof in Appendix B. Theorem 6 states that the discrepancy between $(\mathbf{U}'^{(s)}, \mathbf{V}'^{(s)})$ and $(\mathbf{U}^{(s)}, \mathbf{V}^{(s)})$ exists if the observation is corrupted by additive noise. However, if the noise is small, then the estimation error is small as well. Directly based on Theorem 6, we next find that the local solution can be regarded as the unique solution with additive noise.

Corollary 7 *Let $(\mathbf{U}^{(s)}, \mathbf{V}^{(s)})$ and $(\mathbf{U}'^{(s)}, \mathbf{V}'^{(s)})$ be the unique and local solutions obtained from minimizing \mathcal{O} defined in Eq. (3), respectively, where $\mathbf{U}'^{(s)} = \mathbf{U}^{(s)} + \mathbf{E}_{\mathbf{U}}^{(s)}$, $\mathbf{V}'^{(s)} = \mathbf{V}^{(s)} + \mathbf{E}_{\mathbf{V}}^{(s)}$ for some errors $\mathbf{E}_{\mathbf{U}}^{(s)}$ and $\mathbf{E}_{\mathbf{V}}^{(s)}$. Given some $\epsilon > 0$, there exists a $\delta > 0$ such that if $E_* = O(\delta)$ where E_* is the largest absolute value of $\mathbf{E}_{\mathbf{U}}^{(s)}$ and $\mathbf{E}_{\mathbf{V}}^{(s)}$, then the distance $D_{(\mathbf{U}^{(s)}, \mathbf{V}^{(s)})}(\mathbf{U}'^{(s)}, \mathbf{V}'^{(s)}) < \epsilon$.*

5.3 Generalization error bound

First we define some notations. Let a data point $\mathbf{x} \in \mathcal{H}$, where \mathcal{H} denotes the Hilbert space. The reconstruction error of \mathbf{x} under the NMF framework is defined as $f_{\mathbf{U}}(\mathbf{x}) = \min_{\mathbf{v} \in \mathbb{R}_+^K} \|\mathbf{x} - \mathbf{U}\mathbf{v}^\top\|_2^2$, which is also called the loss function. Given a finite number of independent observations $\mathbf{x}_1, \dots, \mathbf{x}_N$ (the column vectors in \mathbf{X}), the

expected reconstruction error $R(\mathbf{U})$ and the empirical reconstruction error $R_N(\mathbf{U})$ are

$$R(\mathbf{U}) = \int_{\mathbf{x}} f_{\mathbf{U}}(\mathbf{x}) p(\mathbf{x}) d\mathbf{x} \quad \text{and} \quad R_N(\mathbf{U}) = \frac{1}{N} \sum_{i=1}^N f_{\mathbf{U}}(\mathbf{x}_i),$$

where $p(\mathbf{x})$ is the probability density function. The generalization error is defined as the absolute difference between $R(\mathbf{U})$ and $R_N(\mathbf{U})$.

For the WM-NMF algorithm with a learned \mathbf{U} and \mathbf{w} , we can encode a data point \mathbf{x} as a representative vector $\mathbf{v} \in \mathbb{R}_+^K$. We write the generalization error, for independent random variables $\mathbf{x}_1, \dots, \mathbf{x}_n$, as

$$|R(\mathbf{U}) - R_N(\mathbf{U})| = \left| E_{\mathbf{x}} \left\{ \min_{\mathbf{v} \in \mathbb{R}_+^K} \left\| (\mathbf{x} - \mathbf{U}\mathbf{v}^\top) \mathbf{w} \right\|_2^2 \right\} - \frac{1}{N} \sum_{i=1}^N \min_{\mathbf{v} \in \mathbb{R}_+^K} \left\| (\mathbf{x}_i - \mathbf{U}\mathbf{v}^\top) \mathbf{w} \right\|_2^2 \right|.$$

We find below the generalization errors of WM-NMF by the covering number and the Rademacher complexity to measure the complexity of the whole predefined hypothesis class. The generalization error of WM-NMF is expected to be smaller than that of NMF due to the fact that WM-NMF reduces the search space for optimizing \mathbf{U} and the definitions of covering number and Rademacher complexity (Bartlett and Mendelson, 2002). We first show the following dimensionality dependent generalization bound that employs the covering number technique.

Theorem 8 *For the WM-NMF problem, let \mathbf{x}_i be an independent bounded random variable. For any learned normalized \mathbf{U} and $\delta \in (0, 1)$, with probability at least $1 - \delta$, we have*

$$|R(\mathbf{U}) - R_N(\mathbf{U})| \leq \frac{2}{N} + w^{*2} \sqrt{\frac{MK \log \left\{ 4(1+K) \sqrt{MK} N w^{*2} \right\} - \log(\delta/2)}{2N}}$$

where $w^* = \max\{w_1, \dots, w_N\}$ denotes the maximum of weight across N objects from the learned WM-NMF.

According to Theorem 2 of Maurer and Pontil (2010) which employs the Rademacher complexity technique, we have the following dimensionality independent generalization bound. The benefit of the dimensionality independent bound is that the generalization error can be analyzed when the data lies in an infinite or high-dimensional space.

Theorem 9 *For the WM-NMF problem, let \mathbf{x}_i be an independent bounded random variable. For any learned normalized \mathbf{U} and $\delta \in (0, 1)$, with probability at least $1 - \delta$, we have*

$$|R(\mathbf{U}) - R_N(\mathbf{U})| \leq w^* \left(4K \sqrt{\frac{\pi}{N}} + 2K^2 \sqrt{\frac{\pi}{N}} \right) + w^{*2} \sqrt{\frac{\log(1/\delta)}{2N}}$$

where $w^* = \max\{w_1, \dots, w_N\}$ denotes the maximum of weight across N objects from the learned WM-NMF.

Theorems 8 and 9 both imply uniform convergence in probability and are proved under the Vapnik–Chervonenkis learning theory. We provide the proofs for both theorems in Appendix B.

6. Experiments

In this section, we present experimental results on two simulated datasets, one handwritten digit dataset, and one multi-omics dataset. For each dataset, we use six metrics to evaluate the clustering performance: accuracy (ACC), normalized mutual information (NMI), Precision, Recall, F-score, Adjusted Rand index (Adj-RI). ACC measures the proportion of equality between the cluster labels and the true labels. NMI is a normalization of the mutual information, where mutual information measures the agreement of the two clustering assignments, ignoring permutations of cluster labels. The other four metrics are based on the construction of a contingency table between true labels and clustering results. For all these metrics, higher values indicate better clustering performance. Details and formulas of them are available in Manning et al. (2008).

In addition, we compare WM-NMF with several competing multi-view clustering algorithms described below:

1. *K*-means: The default `kmeans` function in MATLAB is implemented to obtain the results. There are two strategies: (1) Apply *K*-means independently on each single view, and select the best performance of *K*-means as the final results. We denote this strategy as BSV-kmeans. (2) Apply *K*-means on the data where all the views are concatenated. We denote this strategy as ConcatK.
2. Spectral clustering: The classical spectral clustering algorithm is applied to the datasets. The default function `spectralcluster` in MATLAB is implemented to obtain the results. Similar to the above *K*-means, we denote BSV-Spectral as the best performance of spectral clustering over each single view, and ConcatSpectral represents the result of spectral clustering on the data with all views concatenated.
3. MultiNMF: Multi-view nonnegative matrix factorization with equal weight. MultiNMF1 is implemented with equal weights summing to 1, i.e., $\alpha_s = 1/n_v$ for $s = 1, \dots, n_v$. MultiNMF2 is implemented with equal weight such that $\alpha_s = 0.01$, which is shown to have the best performance in Liu et al. (2013). The clustering is performed based on \mathbf{V}^* by *K*-means.
4. LRSSC : Low-rank sparse subspace clustering (LRSSC) which is shown to be very competitive in multi-view clustering (Brbić and Kopriva, 2018). More specifically, we implement four variants: P-MLRSSC, C-MLRSSC, P-KMLRSSC

and C-KMLRSSC which represent pairwise, centroid-based, pairwise kernel, and centroid-based kernel multi-view low-rank sparse subspace clustering, respectively.

5. NMF-W: A simplified version of WM-NMF. We denote NMF-W1 as the case when \mathbf{w} is fixed a priori in WM-NMF. Comparing NMF-W1 to WM-NMF, we emphasize the importance of the observation-specific weight. Likewise, we denote NMF-W2 as the situation when \mathbf{w} is fixed and β is set to 0, such that there is no manifold regularization in WM-NMF. Comparing NMF-W2 to WM-NMF, we emphasize the importance of the observation-specific weight and the manifold regularization.

For all the experiments, we set $p = 5$ and $\beta = 0.01$ for WM-NMF and we use the default settings for all the other algorithms.

6.1 Data description

We first summarize all the datasets below and the key information of the datasets are listed in Table 2.

1. **Synthetic dataset 1:** This synthetic dataset is generated by a four-component Gaussian mixture model. The data contains six views, with the first four being uncorrupted and the last two being corrupted. More specifically, we randomly generate the cluster centers, denoted by $\boldsymbol{\mu}_1, \dots, \boldsymbol{\mu}_4$, for views $\mathbf{X}^{(1)}$ to $\mathbf{X}^{(4)}$. Each element of $\boldsymbol{\mu}_j$, $j = 1, \dots, 4$ is independently drawn from the normal distribution with mean randomly generated from a uniform distribution $\mathcal{U}[a, a + 10]$ and variance 1. We set $a = 10, 20, 30, 40$ for these four views. To generate the covariance matrix for each view, we first generate a random number b from $\mathcal{U}[0.1, 1]$, then multiply a symmetric matrix of all ones by b . Lastly, we take element-wise power of this matrix by a symmetric Toeplitz matrix whose diagonals are all 0. The prior proportions of the 4 components are set to be equal and sum to 1. Further, we set $\mathbf{X}^{(5)}$ to be the same as $\mathbf{X}^{(1)}$ but with the first 300 observations added by random noises independently generated from $\mathcal{N}(0, 5)$. We also let $\mathbf{X}^{(6)}$ to be the same as $\mathbf{X}^{(3)}$ but with the first 1000 observations added by random noises independently generated from $\mathcal{N}(0, 10)$. We change N , M , K and n_v to study the computational complexity in Subsection 6.6.
2. **Synthetic dataset 2:** This synthetic dataset contains four views, with the last view being corrupted. We simulate this dataset in a similar way to Synthetic dataset 1. That is, we generate the four views by the Gaussian mixture model. To illustrate the functionality of \mathbf{w} on the heterogeneous data and corrupted data, we generate the second view with larger variance while all the other views with smaller and equal variances. Moreover, we add normal noise with mean 45 and variance 20 to the last 500 observations of the fourth view.

3. **Handwritten digit dataset:** The handwritten digits (0-9) is obtained from the UCI Machine Learning Repository website (Dua and Graff, 2017)¹ and the dataset contains 2000 digits. Each digit can be decomposed into four views: Fourier coefficients of the character shapes (**fou**), pixel averages in 2×3 windows (**pix**), Zernike moments (**zer**) and profile correlations (**fac**). Each view contains 10 labels, i.e., from 0 to 9. To perform clustering analysis, we treat the labels of the digits as unknown and only use the labels to evaluate the clustering performance.
4. **Corrupted handwritten digit dataset:** We modify the original handwritten digit dataset to examine the effectiveness of our proposed observation-specific weighting mechanism when the information content for one view is different for each observation. More specifically, this dataset includes all the views from the above dataset 2. Besides, we modify the third view (**zer**) that the first 500 observations are replaced by random noises generated from Normal with a mean of 300 and standard deviation 50. Thus, we would expect that the third view is not important in terms of clustering from the first 500 observations.
5. **Liver hepatocellular carcinoma (LIHC):** This is a multi-omics dataset used in the application in Seal et al. (2020). Each sample has three different types of measurements (views): gene expression (GE), copy number variation (CNV), and DNA methylation (DNAm). We pre-process the raw data in the same way as in Seal et al. (2020). The processed dataset has 404 samples, and the three views have 15397, 16384, 16384 features, respectively. To further reduce the dimension, we select the top 100 most highly variable features for each view. In addition, these samples belong to either tumor or normal samples, where such class labels are known a priori. Thus, we would expect there are two clusters for this dataset.

6.2 Results on the synthetic datasets

The synthetic dataset 1 represents a scenario where data is well-separated and noise level is small. Figure 9 shows the two-dimensional t-SNE plot (van der Maaten and Hinton, 2008) for each view with individual observation’s color coded by its cluster membership. The clustering results in Table 4 indicate that both WM-NMF and NMF-W1 work the best among all the algorithms while Figure 10 shows WM-NMF’s ability in identifying the corrupted data. Especially, the first 1000 observations have almost zero weights \mathbf{w} for view 6, which is consistent with the simulation setting. Besides, views 1 to 4 are highly similar to each other in terms of the clustering structure, so we expect some of them to dominate the overall contributions to the consensus matrix. Figure 10 shows that view 4 contributes the most. Moreover,

1. <https://archive.ics.uci.edu/ml/datasets/Multiple+Features>

Table 2: Detailed information about the experiment datasets.

| Dataset | view | observations | features | clusters |
|-------------------|--------------------|--------------|----------|----------|
| Synthetic 1 | $\mathbf{X}^{(1)}$ | 5000 | 100 | 10 |
| | $\mathbf{X}^{(2)}$ | 5000 | 150 | 10 |
| | $\mathbf{X}^{(3)}$ | 5000 | 50 | 10 |
| | $\mathbf{X}^{(4)}$ | 5000 | 200 | 10 |
| | $\mathbf{X}^{(5)}$ | 5000 | 100 | - |
| | $\mathbf{X}^{(6)}$ | 5000 | 50 | - |
| Synthetic 2 | $\mathbf{X}^{(1)}$ | 2000 | 100 | 10 |
| | $\mathbf{X}^{(2)}$ | 2000 | 100 | 10 |
| | $\mathbf{X}^{(3)}$ | 2000 | 100 | 10 |
| | $\mathbf{X}^{(4)}$ | 2000 | 100 | - |
| Handwritten digit | fou | 2000 | 76 | 10 |
| | pix | 2000 | 240 | 10 |
| | zer | 2000 | 47 | 10 |
| | fac | 2000 | 216 | 10 |
| LIHC | GE | 404 | 100 | 2 |
| | CNA | 404 | 100 | 2 |
| | DNA _m | 404 | 100 | 2 |

recall that view 5 is designed to be the same as view 1 and view 6 is the same as view 3 except the first 300 and 1000 observations with additive noise. We can see that the weights for each pair are close from the figure. Furthermore, we require the observation weights summing to 1 across all views, so the reduced weights due to corruption from view 6 should be compensated to other views. This evidence can be collected from the first 1000 observations in view 4. We include Figures 9 and 10 and Table 4 in Appendix C.

Next, we analyze the second synthetic data whose clustering structure is more complex. Figure 2 shows the two-dimensional t-SNE visualization of this data for each view with observation’s color coded by its cluster membership. Figure 3 shows the clustering results for all the methods. Note that we do not plot the results LRSSC algorithm because it outputs the average and standard deviation only. Among the four algorithms in LRSSC, we report the highest six metric scores with standard deviations in the bracket as 0.85 (0.06), 0.85 (0.06), 0.82 (0.07), 0.88 (0.05), 0.91 (0.04) and 0.83 (0.07). First, we observe that WM-NMF outperforms other algorithms except the ConcatK in terms of the recall score only. Second, WM-NMF achieves smaller standard deviations than others while retaining higher scores. Lastly, both NMF-W1 and NMF-W2 do not work well, suggesting the importance of including observation-specific weight and the manifold regularization.

The results in Figure 4 match our simulation setting that the last 500 observations in view 4 are corrupted because they have very low observation-specific weights. As

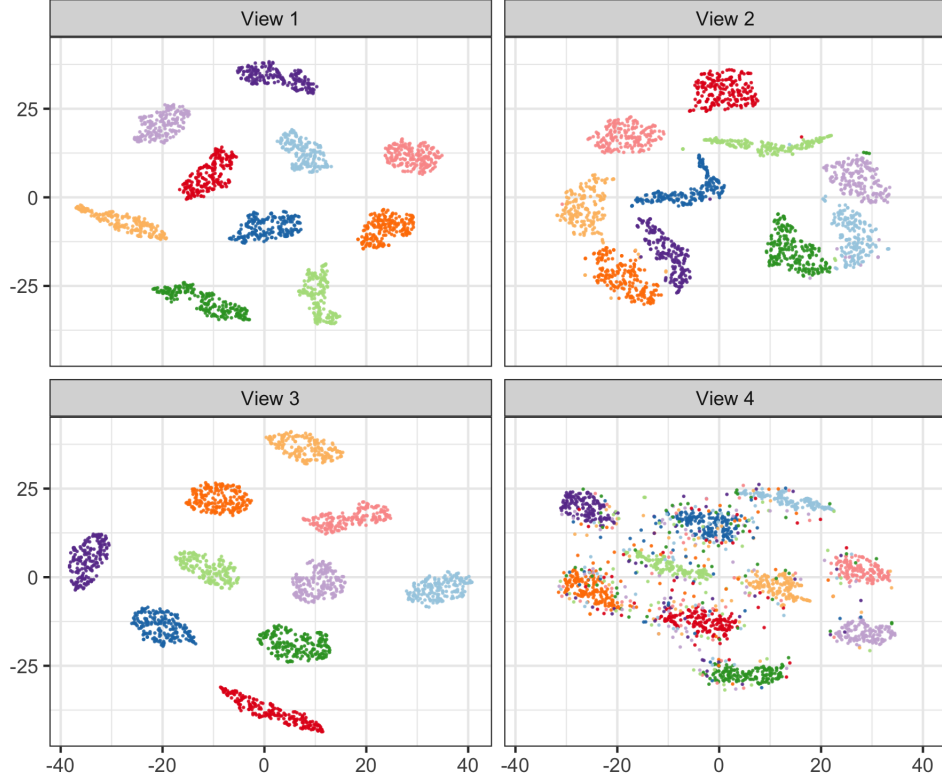


Figure 2: Two-dimensional t-SNE visualization of synthetic dataset 2 for each view. Colors indicate the cluster membership.

described above, view 2 is generated with larger variance, so it should contribute the least to the consensus matrix, which therefore leads to smaller α_2 and \mathbf{w} values. The relatively smaller \mathbf{w} in view 2 can be seen from Figure 4 and the estimated α is 0.28, 0.13, 0.29, 0.30 for the four views respectively. These consolidate the functionality of \mathbf{w} and α and thus make the algorithm robust to corrupted data.

6.3 Results on the handwritten digit dataset

Table 3 compares the result of WM-NMF to the other algorithms based on the handwritten digit dataset. It is worth noting that WM-NMF obtains the highest scores for all six evaluation metrics. All the other competing methods show clustering performance significantly worse than WM-NMF. Now, we analyze the effectiveness of the manifold regularization, view-specific and observation-specific weights, respectively. First, we observe that NMF-W1 performs better than NMF-W2, which implies the importance of the manifold regularization for clustering analysis. Second, WM-NMF, NMF-W1, and NMF-W2 all outperform MultiNMF, this shows the ineffectiveness of using equal weight for α . Third, we find that WM-NMF hits higher scores than

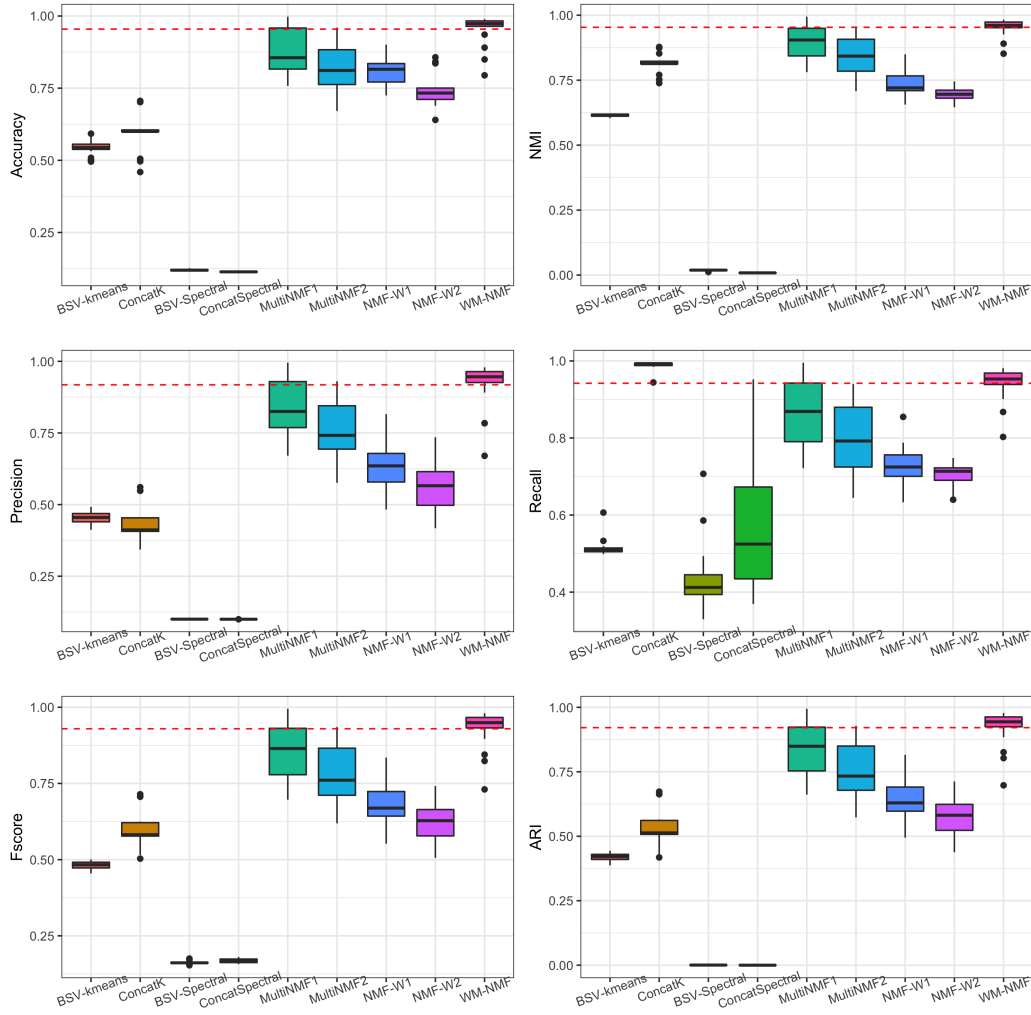


Figure 3: Boxplots representing clustering results for the synthetic dataset 2 based on 20 replications for each algorithm.

NMF-W1. This demonstrates the advantage of using observation-specific weight and the ability of WM-NMF on integrating heterogeneous data.

For the corrupted digit dataset, which includes a corrupted view, the MultiNMF2 algorithm obtains relatively low accuracy (72%) and low normalized mutual information (70%). The four algorithms of low-rank sparse subspace clustering (LRSSC) is demonstrated to have the ability of dealing with corrupted data. Particularly, P-KMLRSSC algorithm obtains the accuracy of 78% and the adjusted rand index of 73%. Nevertheless, the proposed WM-NMF algorithm still outperforms the LRSSC algorithms with ACC (95%), NMI (93%), Precision (90%), Recall (93%), F-score (92%) and Adj-RI (91%). This further verifies that WM-NMF is powerful in alleviating the negative effects of corrupted views.

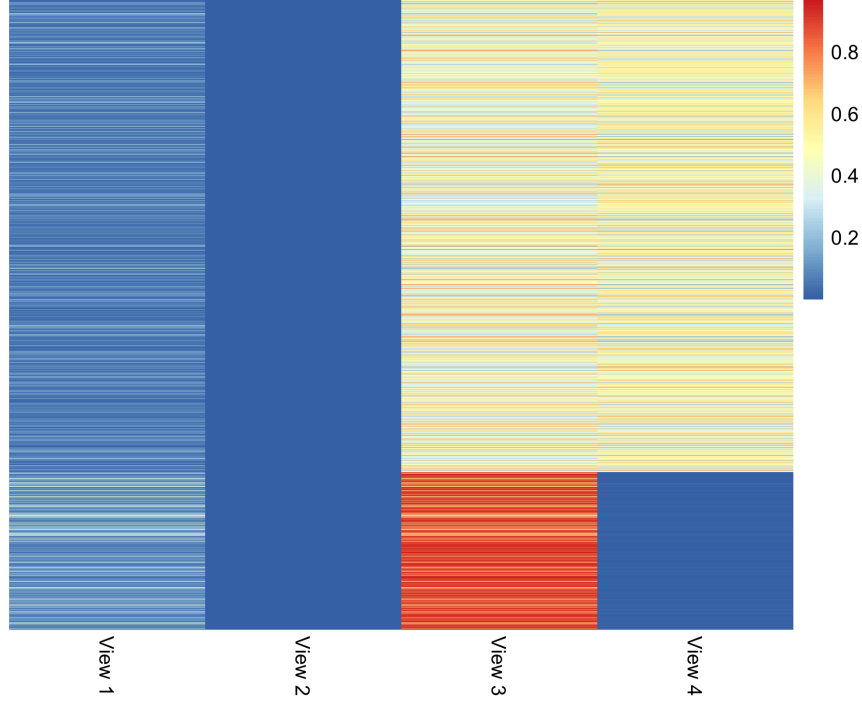


Figure 4: Heatmap for the observation weights \mathbf{w} of the synthetic dataset 2. The x-axis measures the view index and the y-axis from top to bottom represents observation 1 to observation 2000.

Compared to NMF-W1 and NMF-W2 which can also assign small weights to the corrupted views, WM-NMF has higher evaluation metric scores because it further assigns lower weights to the specific corrupted observations. This evidence can be collected from Figure 5, which depicts that the first 500 observations from the third view are weighted around 0, which matches with the true data. Moreover, comparing the corrupted to the uncorrupted digit data, we find that scores of WM-NMF almost keep unchanged while those of NMF-W1 and NM-W2 drop significantly. Overall, this corrupted digit dataset again confirms the effectiveness of WM-NMF in dealing with corrupted data and in improving the clustering performance when corrupted data exist.

6.4 Results on the LIHC dataset

It is found that several factors such as copy number variation (CNV) and DNA methylation (DNAm) affect gene expression (GE) and they work interweavingly during tumor growth and progression (You and Jones, 2012). Seal et al. (2020) uses both CNV and DNAm to predict the sample status, either tumor or normal sample, so it is treated as a classification problem and the accuracy is 95.1%. In this paper, we treat

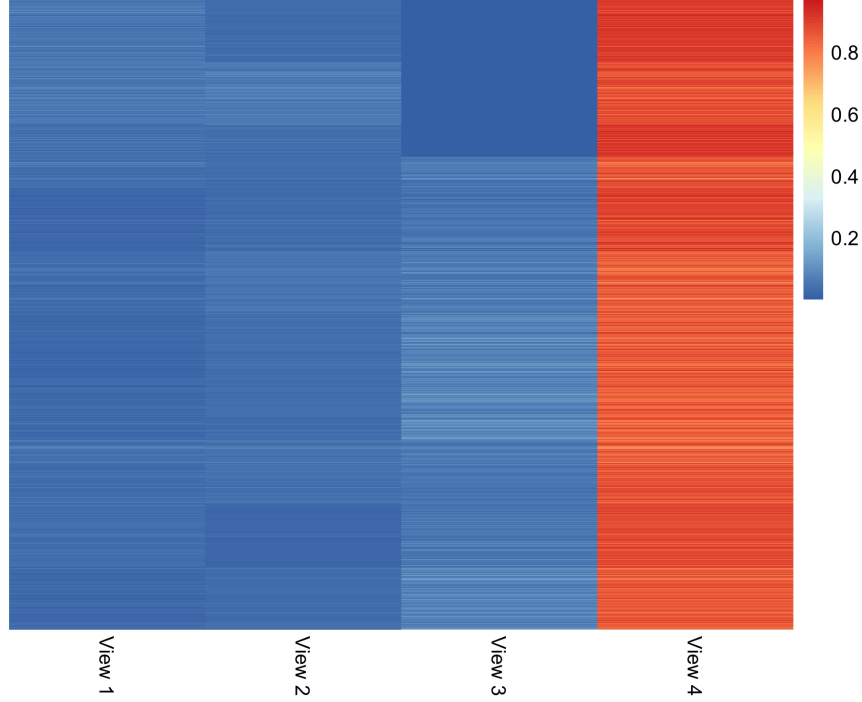


Figure 5: Heatmap for the observation-specific weights \mathbf{w} of the corrupted digit dataset. The x-axis measures the view index and the y-axis from top to bottom represents observation 1 to observation 2000.

this data as unsupervised problem and integrate all the three omics data to conduct clustering analysis.

Figure 6 presents the analysis results. As it shows, both WM-NMF and NMF-W2 outperform the other algorithms in all the evaluation metrics while WM-NMF behaves much better than NMF-W2. The average scores of the proposed WM-NMF for the 6 evaluation metrics are 0.97, 0.70, 0.99, 0.95, 0.97, and 0.83, respectively. Note that we do not plot the results LRSSC algorithm because it outputs the average and standard deviation only. Among the four algorithms in LRSSC, we report the highest six metric scores with standard deviations in the bracket as 0.57 (0.04), 0.18 (0.00), 0.88 (0.00), 0.54 (0.00), 0.67 (0.00) and 0.10 (0.00). Besides, the proposed WM-NMF algorithm has lower standard deviations compared to all the other algorithms. It is worth noting that the clustering algorithm WM-NMF achieves slightly higher accuracy than the neural network approach for classification in Seal et al. (2020).

6.5 Empirical analysis on the tuning parameters

In this section, we show how to select p , β , and K using the synthetic dataset 1 and the handwritten digit dataset. The default values are $p = 5$, $\beta = 0.01$, and $K = 10$. During the experiment, we change the target parameter and fix the remaining ones.

Table 3: Comparisons of clustering performance between WM-NMF and other competing methods for both versions of the handwritten digit dataset. Numbers in the bracket represent standard deviations of the corresponding scores, which is obtained based on 20 replications for each algorithm. The top performances are in blue.

| Data | Algorithm | ACC | NMI | Precision | Recall | F-score | Adj-RI |
|------------------|----------------|-------------|-------------|-------------|-------------|-------------|-------------|
| Digits | BSV-kmeans | 0.69 (0.07) | 0.70 (0.03) | 0.61 (0.05) | 0.67 (0.04) | 0.63 (0.05) | 0.59 (0.05) |
| | ConcatK | 0.63 (0.07) | 0.62 (0.03) | 0.51 (0.05) | 0.59 (0.03) | 0.55 (0.04) | 0.49 (0.04) |
| | BSV-Spectral | 0.68 (0.00) | 0.71 (0.00) | 0.58 (0.00) | 0.68 (0.00) | 0.62 (0.00) | 0.58 (0.00) |
| | ConcatSpectral | 0.12 (0.00) | 0.01 (0.00) | 0.10 (0.00) | 0.41 (0.04) | 0.16 (0.00) | 0.00 (0.00) |
| | MultiNMF1 | 0.64 (0.03) | 0.58 (0.02) | 0.51 (0.03) | 0.54 (0.03) | 0.52 (0.03) | 0.47 (0.03) |
| | MultiNMF2 | 0.79 (0.04) | 0.72 (0.02) | 0.66 (0.03) | 0.69 (0.03) | 0.68 (0.03) | 0.64 (0.03) |
| | P-MLRSSC | 0.75 (0.07) | 0.77 (0.04) | 0.68 (0.07) | 0.75 (0.05) | 0.71 (0.06) | 0.68 (0.07) |
| | C-MLRSSC | 0.75 (0.06) | 0.77 (0.04) | 0.68 (0.06) | 0.74 (0.05) | 0.71 (0.06) | 0.67 (0.06) |
| | P-KMLRSSC | 0.77 (0.06) | 0.72 (0.02) | 0.66 (0.05) | 0.68 (0.05) | 0.67 (0.04) | 0.63 (0.05) |
| | C-KMLRSSC | 0.76 (0.07) | 0.72 (0.03) | 0.65 (0.06) | 0.68 (0.05) | 0.67 (0.05) | 0.63 (0.06) |
| | NMF-W1 | 0.92 (0.03) | 0.88 (0.03) | 0.85 (0.06) | 0.88 (0.03) | 0.86 (0.05) | 0.84 (0.05) |
| | NMF-W2 | 0.81 (0.08) | 0.77 (0.05) | 0.69 (0.10) | 0.76 (0.06) | 0.72 (0.08) | 0.69 (0.09) |
| | WM-NMF | 0.96 (0.02) | 0.93 (0.01) | 0.93 (0.04) | 0.94 (0.01) | 0.93 (0.03) | 0.93 (0.03) |
| Corrupted digits | BSV-kmeans | 0.69 (0.07) | 0.70 (0.03) | 0.61 (0.05) | 0.67 (0.04) | 0.63 (0.05) | 0.59 (0.05) |
| | ConcatK | 0.63 (0.07) | 0.66 (0.02) | 0.51 (0.06) | 0.61 (0.03) | 0.56 (0.04) | 0.50 (0.05) |
| | BSV-Spectral | 0.68 (0.00) | 0.71 (0.00) | 0.58 (0.00) | 0.68 (0.00) | 0.62 (0.00) | 0.58 (0.00) |
| | ConcatSpectral | 0.12 (0.00) | 0.01 (0.00) | 0.10 (0.00) | 0.48 (0.14) | 0.16 (0.00) | 0.00 (0.00) |
| | MultiNMF1 | 0.78 (0.04) | 0.70 (0.02) | 0.65 (0.04) | 0.67 (0.03) | 0.66 (0.03) | 0.62 (0.03) |
| | MultiNMF2 | 0.78 (0.05) | 0.78 (0.02) | 0.69 (0.05) | 0.76 (0.03) | 0.72 (0.04) | 0.69 (0.05) |
| | P-MLRSSC | 0.78 (0.07) | 0.75 (0.07) | 0.72 (0.07) | 0.79 (0.06) | 0.81 (0.05) | 0.73 (0.08) |
| | C-MLRSSC | 0.76 (0.09) | 0.75 (0.07) | 0.71 (0.08) | 0.79 (0.05) | 0.81 (0.04) | 0.72 (0.08) |
| | P-KMLRSSC | 0.59 (0.04) | 0.50 (0.03) | 0.49 (0.04) | 0.51 (0.03) | 0.59 (0.03) | 0.44 (0.04) |
| | C-KMLRSSC | 0.63 (0.04) | 0.53 (0.02) | 0.51 (0.02) | 0.55 (0.02) | 0.62 (0.01) | 0.48 (0.02) |
| | NMF-W1 | 0.82 (0.06) | 0.80 (0.03) | 0.70 (0.08) | 0.79 (0.04) | 0.74 (0.06) | 0.71 (0.07) |
| | NMF-W2 | 0.72 (0.06) | 0.70 (0.04) | 0.58 (0.07) | 0.69 (0.05) | 0.62 (0.06) | 0.58 (0.07) |
| | WM-NMF | 0.95 (0.04) | 0.93 (0.02) | 0.90 (0.07) | 0.93 (0.02) | 0.92 (0.05) | 0.91 (0.05) |

We first analyze the effect of p on the algorithm performance. Figure 7 shows how the metric scores and the distribution of weights change as p changes. For the experiments, we let $p \in \{2, 4, 5, 8, 11\}$. The left panel shows p controls the sparsity of the weight vector, i.e., the effect of different values of p on the distributions of the weight vector. As p decreases, the weight vector α becomes sparser, which is consistent with Theorem 2. The right panel shows that all the metric scores are close with $p \in \{4, 5, 8, 11\}$ (a moderate size).

Next we empirically illustrate how to choose β , the manifold regularizer. Before algorithm implementation, entries in \mathbf{X} are scaled so that the value \mathcal{O}_1 is in general small. Consequently, we tend to choose a small β to balance the matrix factorization effect and the manifold regularization effect. As we can see from Figure 11, both

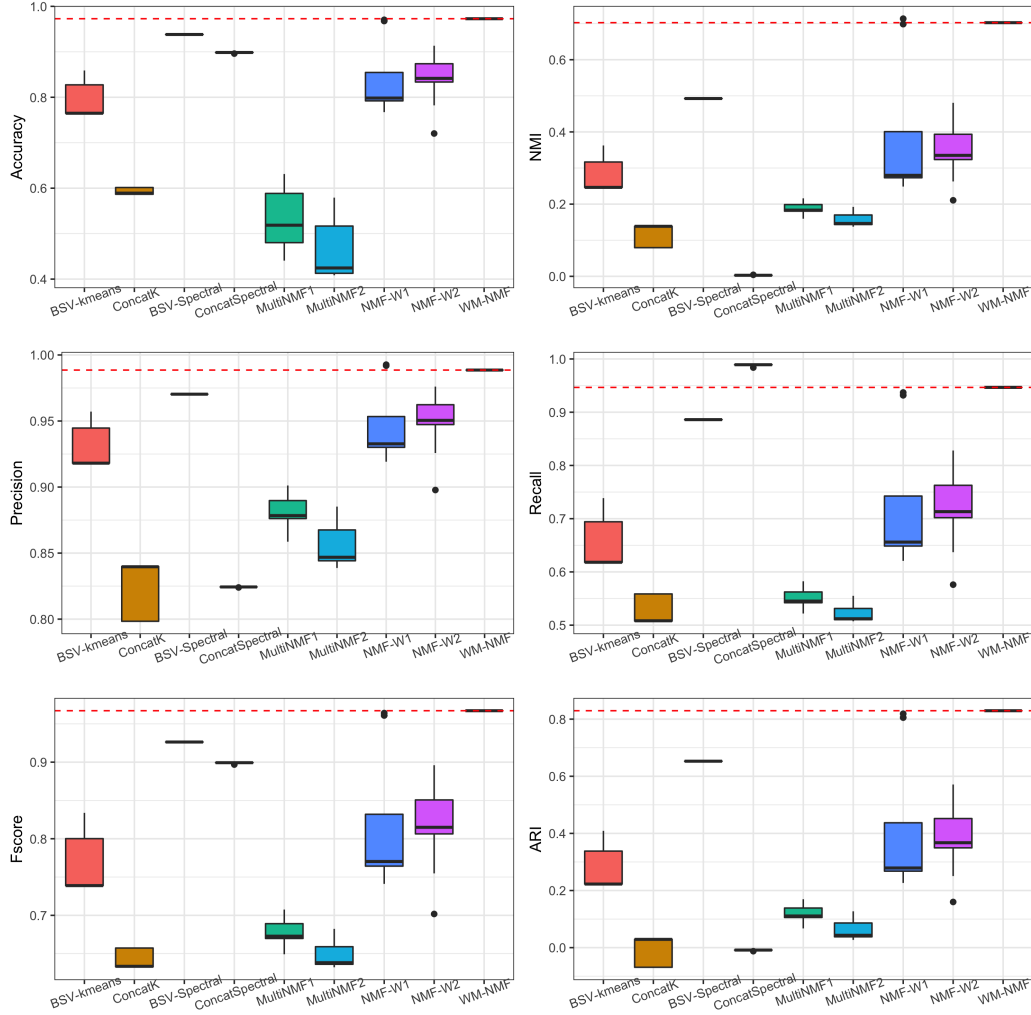


Figure 6: Boxplots representing clustering results for LIHC dataset based on 20 replications for each algorithm. The dashed red line is the average score of WM-NMF.

datasets demonstrate robust results with different values of β . This implies that the clustering performance is robust to relatively small β values. Finally, we empirically show how to choose K . As we can see from Figure 12, both datasets demonstrate robust results when K lies in a neighbour of the ground truth. This means that the choice of K may not affect the clustering results even though it is overestimated or underestimated. We include Figures 11 and 12 in Appendix C.

6.6 Complexity and convergence study

To study the computational complexity, we run a series of experiments on a server with 10 processors and each processor (2.2 GHz Intel Xeon) uses 20GB memory. We

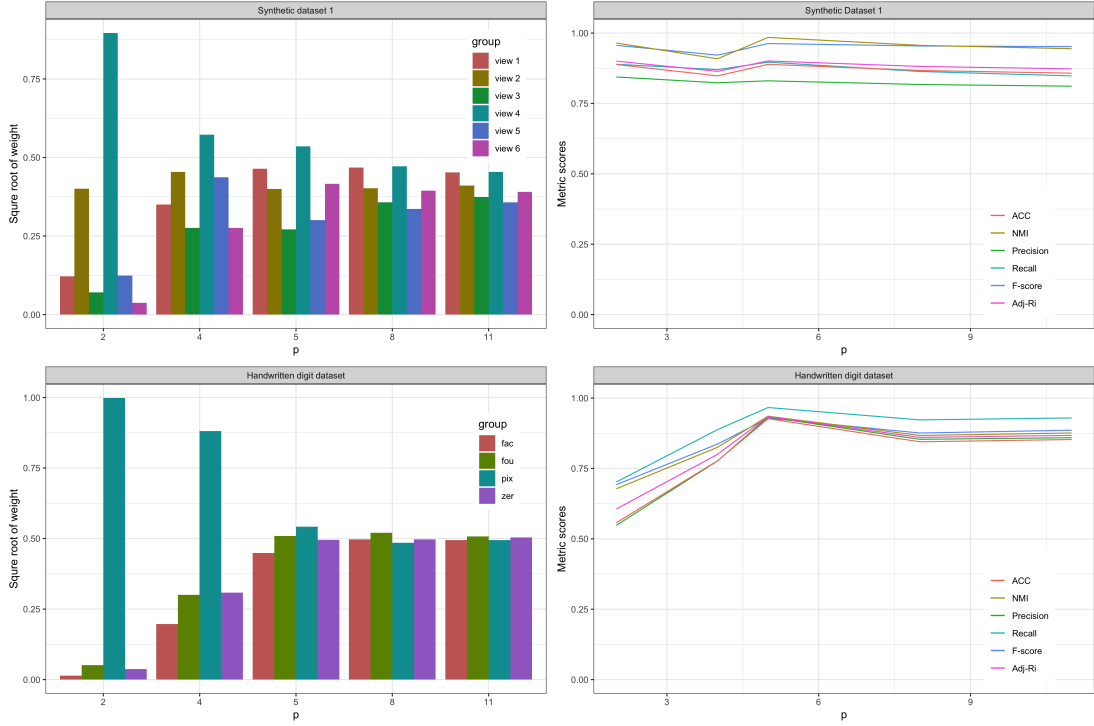


Figure 7: Distributions of view-specific weight α (left) and the metric scores (right) under different values of p for the synthetic dataset 1 and handwritten digit dataset.

change N and n_v to investigate the corresponding effects. The default setting is 5000 data points ($N = 5000$), 4 views ($n_v = 4$) with 10 clusters ($K = 10$) and 100 features ($M = 100$). During the experiment, we change one aspect while keeping all others fixed. The values of N are set to 3k, 5k, 7k, 9k, and 11k, which is larger than M , so the theoretical complexity should be quadratic in N . We find the running time is overall linear in terms of smaller N and scales well for large N (e.g. $N > 9000$). Even though the theoretical result for $N > M$ indicates quadratic complexity in N , the running time is still acceptable. For n_v , we set its value from 2 to 6. Column 1 of Figure 8 shows the running time is linear in n_v and matches the complexity analysis in Section 4.8.

The multiplicative update rule for minimizing the objective function \mathcal{O} is iterative. Theorem 5 shows that the algorithm for updating \mathbf{U} and \mathbf{V} can converge to a local solution. Here we investigate how fast the convergence is empirically. Columns 2–3 of Figure 8 demonstrate the convergence curves on all datasets. The x-axis is the number of iterations and y-axis is the objective function value. We see that the algorithm converges very fast, usually within 50 iterations for all datasets.

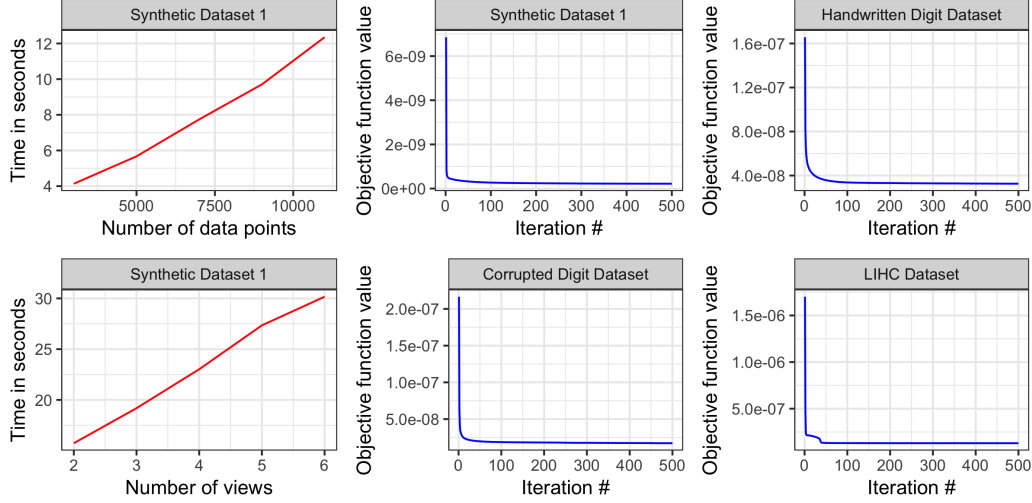


Figure 8: Running time of the WM-NMF algorithm on the synthetic dataset 1 (column 1); convergence curves of WM-NMF algorithm on the synthetic dataset 1, handwritten digit dataset, corrupted digit dataset, and LIHC dataset (columns 2–3).

7. Discussion

We have developed a weighted multi-view NMF (WM-NMF) algorithm, with the goal of learning multi-view data for integrative clustering analysis. One key feature of WM-NMF is the ability to learn both view-specific and observation-specific weights to quantify each view’s information content. Thus, the unnecessary views’ adverse effects can be alleviated and the positive effects of the important views are enlarged, making WM-NMF robust to the potentially heterogeneous multi-view data. Such ability enables WM-NMF to deal with heterogeneous and corrupted data. In this paper, we studied the property of the introduced weighting scheme for integrating multi-view data under the NMF framework. Technically, our proposed weighting scheme can be integrated into other methods such as model-based approach. In practice, different views often consist of variables from different domains, such as being continuous, categorical, and count-valued, so a mixed model with the proposed weighting scheme can be potentially used to handle the mixed multi-view data jointly.

Appendix A

In this section, we provide the derivations for updates of $\mathbf{U}^{(s)}$, $\mathbf{V}^{(s)}$, and α_s . Besides, we provide the details on how to count the operation counts summarized in Table 1.

Update of $\mathbf{U}^{(s)}$ and $\mathbf{V}^{(s)}$

With the notations in the main text, we have

$$\frac{\partial \mathcal{O}_1}{\partial u_{ik}} = 2 [\mathbf{U}\mathbf{V}^\top \text{Diag}^2(\mathbf{w})\mathbf{V}]_{ik} - 2 [\mathbf{X}\text{Diag}^2(\mathbf{w})\mathbf{V}]_{ik} + \alpha_s^p P_{ik} + \Psi_{ik},$$

where $P_{ik} = 2 \left(\sum_{l=1}^M u_{lk} \sum_{j=1}^N v_{jk}^2 - \sum_{j=1}^N v_{jk} v_{jk}^* \right)$ and Ψ_{ik} is the Lagrange multiplier for the constraint $u_{ik} \geq 0$. Using the complementary slackness condition $\Psi_{ik} u_{ik} = 0$, plugging the expression P_{ik} into Eq. (7) and setting it to 0, we have

$$\begin{aligned} & [\mathbf{U}\mathbf{V}^\top \text{Diag}^2(\mathbf{w})\mathbf{V}]_{ik} u_{ik} - [\mathbf{X}\text{Diag}^2(\mathbf{w})\mathbf{V}]_{ik} u_{ik} + \alpha_s^p \left(\sum_{l=1}^M u_{lk} \sum_{j=1}^N v_{jk}^2 - \sum_{j=1}^N v_{jk} v_{jk}^* \right) u_{ik} = 0 \\ \Leftrightarrow & [\mathbf{U}\mathbf{V}^\top \text{Diag}^2(\mathbf{w})\mathbf{V}]_{ik} u_{ik} + \alpha_s^p \sum_{l=1}^M u_{lk} \sum_{j=1}^N v_{jk}^2 u_{ik} = [\mathbf{X}\text{Diag}^2(\mathbf{w})\mathbf{V}]_{ik} u_{ik} + \alpha_s^p \sum_{j=1}^N v_{jk} v_{jk}^* u_{ik}. \end{aligned}$$

Similarly for $\mathbf{V}^{(s)}$, we have

$$\frac{\partial \mathcal{O}_2}{\partial v_{jk}} = [\text{Diag}^2(\mathbf{w})\mathbf{V}\mathbf{U}^\top \mathbf{U}]_{jk} - [\text{Diag}^2(\mathbf{w})\mathbf{X}^\top \mathbf{U}]_{jk} + \alpha_s^p [\mathbf{V}\mathbf{Q}\mathbf{Q}^\top - \mathbf{V}^* \mathbf{Q}^\top]_{jk} + \beta [\mathbf{L}\mathbf{V}]_{jk} + \Phi_{jk} = 0$$

\Downarrow

$$[\text{Diag}^2(\mathbf{w})\mathbf{V}\mathbf{U}^\top \mathbf{U}]_{jk} + \alpha_s^p [\mathbf{V}\mathbf{Q}\mathbf{Q}^\top]_{jk} + \beta [D\mathbf{V}]_{jk} + \Phi_{jk} = [\text{Diag}^2(\mathbf{w})\mathbf{X}^\top \mathbf{U}]_{jk} + \alpha_s^p [\mathbf{V}^* \mathbf{Q}^\top]_{jk} + \beta [\mathbf{A}\mathbf{V}]_{jk},$$

Multiplying the above equation by v_{jk} and using the complementary slackness condition $\Phi_{jk} v_{jk} = 0$ gives the result.

Update of α_s

When $p > 1$, setting the derivative of \mathcal{O} that only contains α_s with respect to α_s to 0, we get

$$p\alpha_s^{(p-1)} A + \lambda_1 = 0 \quad \Rightarrow \quad \alpha_s = \left(-\frac{\lambda_1}{pA} \right)^{\frac{1}{p-1}},$$

where we assume $A^{(s)} = \|\mathbf{V}^{(s)}\mathbf{Q}^{(s)} - \mathbf{V}^*\|_F^2 > 0$. Given the constraint that $\sum_{s'=1}^{n_v} \alpha_{s'} = 1$, we have

$$\sum_{s'=1}^{n_v} \left(-\frac{\lambda_1}{pA^{(s')}} \right)^{\frac{1}{p-1}} = 1 \quad \Rightarrow \quad (-\lambda_1)^{\frac{1}{p-1}} = \frac{1}{\sum_{s'=1}^{n_v} \left(\frac{1}{pA^{(s')}} \right)^{\frac{1}{p-1}}},$$

Finally, we obtain the solution of α_s

$$\hat{\alpha}_s = \frac{1}{\sum_{s'=1}^{n_v} \left(\frac{A^{(s)}}{A^{(s')}} \right)^{\frac{1}{p-1}}} = \frac{1}{\sum_{s'=1}^{n_v} \left(\frac{\|\mathbf{V}^{(s)} \mathbf{Q}^{(s)} - \mathbf{V}^*\|_F^2}{\|\mathbf{V}^{(s')} \mathbf{Q}^{(s')} - \mathbf{V}^*\|_F^2} \right)^{\frac{1}{p-1}}}.$$

Algorithm operation counts in Table 1

For the update of $\mathbf{U}^{(s)}$, we note that the direct computation of $\mathbf{X}^{(s)} \text{Diag}(\mathbf{w}^{(s)}) \mathbf{V}^{(s)}$ has time $O(M_s N^2 + M_s N K) = O(M_s N^2)$ for multiplication. To reduce the computational complexity of this term, we first square each diagonal entries of $\text{Diag}(\mathbf{w}^{(s)})$ to obtain $\text{Diag}^2(\mathbf{w}^{(s)})$, then multiply the diagonal entries to the corresponding columns of $\mathbf{X}^{(s)}$, and finally multiply $\mathbf{V}^{(s)}$. The resulting complexity for multiplication is $O(M_s N K)$, and therefore it reduces the running time since $N > K$ is typically satisfied in the application of clustering analysis. The second term on the numerator has time $O(NK)$. For the first term on the denominator in Eq. (5), we use the same technique for $\text{Diag}^2(\mathbf{w}^{(s)})$ as mentioned above and compute in such order $\mathbf{U}^{(s)} \left[\mathbf{V}^{(s)\top} \text{Diag}^2(\mathbf{w}^{(s)}) \right] \mathbf{V}^{(s)}$, which results in a time $O(M_s N K)$. The second term on the denominator has time $O(NK + 2K)$. The addition procedure is much easier to count. The addition complexities for the four terms in Eq. (5) are $O(K M_s N)$, $O(NK)$, $O(M_s N K)$, and $O(K M_s + K N)$, respectively.

For the update of $\mathbf{V}^{(s)}$, we compute $\text{Diag}^2(\mathbf{w}^{(s)})$ the same as above and compute $\mathbf{Q}^{(s)} \mathbf{Q}^{(s)\top}$ first in a similar way to $\text{Diag}^2(\mathbf{w}^{(s)})$, so the complexities of the six term in Eq. (6) for the multiplication procedure are $O(N M_s K)$, $O(NK)$, $O(N^2 K)$, $O(N M_s K)$, $O(NK)$ and $O(NK)$, respectively. For the addition procedure, we multiply the diagonal entries of $\mathbf{Q}^{(s)}$ and $\mathbf{Q}^{(s)} \mathbf{Q}^{(s)\top}$ to the corresponding columns of \mathbf{V}^* and $\mathbf{V}^{(s)}$, respectively, so no additions are involved. The complexities are $O(N M_s K)$, $O(N^2 K)$, $O(N M_s K)$ and $O(N^2 K)$, respectively.

The division procedures for $\mathbf{U}^{(s)}$ and $\mathbf{V}^{(s)}$ have time $O(M_s K)$ and $O(NK)$, respectively.

Appendix B

In this section, we provide the proofs for Theorems 1, 5, 6, 8, and 9.

Proof of Theorem 1

Proof First we assume that the denominators in Eq. (5) and (6) are always well-defined.

Remark 10 *The update rules by Lee and Seung (2001) are not well-defined if the denominators are 0. This may happen in a very rare case when all the terms on the denominators are 0. In such case, a small positive number can be added to avoid 0 (Lin, 2007). When it is added, the analyses keep the same, so we stick to the situations without the small positive number in this paper.*

When $t = 1$, Theorem 1 holds by the assumption of this theorem. For $t > 1$, we prove by induction. We first prove for the case of \mathbf{U} . Assuming the results are true at t th iteration, we note that from t to $t + 1$, the step size for updating u_{ik} in Eq. (5) is positive:

$$\frac{u_{ik}}{[\mathbf{U}\mathbf{V}^\top \text{Diag}^2(\mathbf{w})\mathbf{V}]_{ik} + \alpha_s^p \sum_{l=1}^M u_{lk} \sum_{j=1}^N v_{jk}^2} > 0.$$

We now consider two situations for the derivative $\nabla_U \mathcal{O}_1$:

Case 1: When $\nabla_U \mathcal{O}_1 = 0$, $u_{ik}^{t+1} = u_{ik}^t$ and it converges as the complementary slackness condition suggests.

Case 2: When $\nabla_U \mathcal{O}_1 \neq 0$,

$$\begin{aligned} u_{ik} &\leftarrow u_{ik} - \frac{u_{ik}}{[\mathbf{U}\mathbf{V}^\top \text{Diag}^2(\mathbf{w})\mathbf{V}]_{ik} + \alpha_s^p \sum_{l=1}^M u_{lk} \sum_{j=1}^N v_{jk}^2} \times \frac{1}{2} \nabla_U \mathcal{O}_1 \\ &= u_{ik} - u_{ik} \frac{\frac{1}{2} \nabla_U \mathcal{O}_1}{[\mathbf{U}\mathbf{V}^\top \text{Diag}^2(\mathbf{w})\mathbf{V}]_{ik} + \alpha_s^p \sum_{l=1}^M u_{lk} \sum_{j=1}^N v_{jk}^2} \\ &= u_{ik} - u_{ik} \left(1 - \frac{[\mathbf{X}\text{Diag}^2(\mathbf{w})\mathbf{V}]_{ik} + \alpha_s^p \sum_{j=1}^N v_{jk} v_{jk}^*}{[\mathbf{U}\mathbf{V}^\top \text{Diag}^2(\mathbf{w})\mathbf{V}]_{ik} + \alpha_s^p \sum_{l=1}^M u_{lk} \sum_{j=1}^N v_{jk}^2} \right) \\ &> 0. \end{aligned}$$

The inequality follows the definition of $\nabla_U \mathcal{O}_1$. When $\nabla_U \mathcal{O}_1 > 0$, the term in the bracket is between 0 and 1. When $\nabla_U \mathcal{O}_1 < 0$, the term in the bracket is negative. Both imply that $u_{ik}^{t+1} > 0$. The proof for $v_{jk}^t, \forall t \geq 1$ is the same as the proof for \mathbf{U} and we omit it here. \blacksquare

Proof of Theorem 5

Proof The updates for \mathbf{V}^* and α_s give exact solutions for the minimization of \mathcal{O} when others are fixed. Therefore, we only need to prove that \mathcal{O} is nonincreasing under the update rules of $\mathbf{U}^{(s)}$ and $\mathbf{V}^{(s)}$, $s = 1, \dots, n_v$. Again to ease the notation without confusion, we drop (s) from the notations, and we simply write \mathbf{V} and \mathbf{U} to refer to a specific view.

The proof is established by defining an auxiliary function and showing the Taylor-expansion of the objective function is less than or equal to the auxiliary function. The update rules are element-wise, and we only need to show L_{ik} and J_{jk} are nonincreasing for Equations (5) and (6), where L_{ik} and J_{jk} denote the part of \mathcal{O} relative to u_{ik} and v_{jk} only, respectively. They are the same as \mathcal{O}_1 and \mathcal{O}_2 as defined above. For u_{ik} , if we define the function

$$\begin{aligned} G(u_{ik}, u_{ik}^t) &= L_{ik}(u_{ik}^t) + L'_{ik}(u_{ik}^t)(u_{ik} - u_{ik}^t) \\ &+ \left\{ \frac{(\mathbf{U}^t \mathbf{V}^T \text{Diag}^2(\mathbf{w})\mathbf{V})_{ik}}{u_{ik}^t} + \frac{\alpha_s^p \sum_{i=1}^M u_{ik}^t \sum_{j=1}^N v_{jk}^2}{u_{ik}^t} \right\} (u_{ik} - u_{ik}^t)^2, \end{aligned}$$

then we have $G(u_{ik}, u_{ik}) = L_{ik}(u_{ik})$.

Next, we need to show $G(u_{ik}, u_{ik}^t) \geq L_{ik}(u_{ik})$. The Taylor expansion of $L_{ik}(u_{ik})$ gives

$$L_{ik}(u_{ik}) = L_{ik}(u_{ik}^t) + L'_{ik}(u_{ik}^t)(u_{ik} - u_{ik}^t) + \frac{1}{2}L''_{ik}(u_{ik}^t)(u_{ik} - u_{ik}^t)^2,$$

with the second order derivative $L''_{ik}(u_{ik}) = 2[\mathbf{V}^T \text{Diag}^2(\mathbf{w})\mathbf{V}]_{kk} + 2\alpha_s^p \sum_{j=1}^N v_{jk}^2$. Comparing the Taylor-expansion of $L_{ik}(u_{ik})$ to $G(u_{ik}, u_{ik}^t)$, we only need to show

$$\frac{\{\mathbf{U}^t \mathbf{V}^T \text{Diag}^2(\mathbf{w})\mathbf{V}\}_{ik}}{u_{ik}^t} + \frac{\alpha_s^p \sum_{i=1}^M u_{ik}^t \sum_{j=1}^N v_{jk}^2}{u_{ik}^t} \geq \{\mathbf{V}^T \text{Diag}^2(\mathbf{w})\mathbf{V}\}_{kk} + \alpha_s^p \sum_{j=1}^N v_{jk}^2.$$

This is easy to verify by comparing the first and second terms of the above inequality, respectively. We have, according to the nonnegative constraints on \mathbf{U} and \mathbf{V}

$$\{\mathbf{U}^t \mathbf{V}^T \text{Diag}^2(\mathbf{w})\mathbf{V}\}_{ik} = \sum_l^K u_{il}^t [\text{Diag}^2(\mathbf{w})\mathbf{V}]_{lk} \geq u_{ik}^t \{\mathbf{V}^T \text{Diag}^2(\mathbf{w})\mathbf{V}\}_{kk},$$

$$\alpha_s^p \sum_{i=1}^M u_{ik}^t \sum_{j=1}^N v_{jk}^2 \geq \alpha_s^p u_{ik}^t \sum_{j=1}^N v_{jk}^2.$$

Thus, $G(u_{ik}, u_{ik}^t)$ is an auxiliary function of $L_{ik}(u_{ik})$. Replacing $G(h, h^t)$ in Eq. (10) by $G(u_{ik}, u_{ik}^t)$, we have

$$\begin{aligned} u_{ik}^{t+1} &= u_{ik}^t - u_{ik}^t \frac{L'_{ik}(u_{ik}^t)}{2[\mathbf{U}\mathbf{V}^T \text{Diag}^2(\mathbf{w})\mathbf{V}]_{ik} + 2\alpha_s^p \sum_{l=1}^M u_{lk} \sum_{j=1}^N v_{jk}^2} \\ &= u_{ik}^t \frac{[\mathbf{X} \text{Diag}^2(\mathbf{w})\mathbf{v}]_{ik} + \alpha_s^p \sum_{j=1}^N v_{jk} v_{jk}^*}{[\mathbf{U}\mathbf{V}^T \text{Diag}^2(\mathbf{w})\mathbf{V}]_{ik} + \alpha_s^p \sum_{l=1}^M u_{lk} \sum_{j=1}^N v_{jk}^2}. \end{aligned}$$

The result follows Lemma 4 that L_{ik} is nonincreasing under the iteration $h^{t+1} = \arg \min_h G(h, h^t)$.

Similar statements for the proof of v_{jk} can be established by defining the auxiliary function

$$\begin{aligned} G(v_{jk}, v_{jk}^t) &= J_{jk}(v_{jk}^t) + J'_{jk}(v_{jk}^t)(v_{jk} - v_{jk}^t) \\ &+ \left\{ \frac{[\text{Diag}^2(\mathbf{w})\mathbf{V}^t \mathbf{U}^T \mathbf{U}]_{jk} + \alpha_s^p [\mathbf{V}^t \mathbf{Q} \mathbf{Q}^T]_{jk} + \beta [\mathbf{D} \mathbf{V}^t]_{jk}}{v_{jk}^t} \right\} (v_{jk} - v_{jk}^t)^2. \end{aligned}$$

It is easy to see $G(v_{jk}, v_{jk}) = J_{jk}(v_{jk})$ and the remaining part is to show $G(v_{jk}, v_{jk}^t) \geq J_{jk}(v_{jk})$. The Taylor-expansion of $J_{jk}(v_{jk})$ gives

$$J_{jk}(v_{jk}) = J_{jk}(v_{jk}^t) + J'_{jk}(v_{jk}^t)(v_{jk} - v_{jk}^t) + \frac{1}{2}J''_{jk}(v_{jk}^t)(v_{jk} - v_{jk}^t)^2,$$

with the second order derivative $J''_{jk}(v_{jk}) = 2 [\text{Diag}^2(\mathbf{w})]_{jj} [\mathbf{U}^\top \mathbf{U}]_{kk} + 2\alpha_s^p \mathbf{Q} \mathbf{Q}^\top + 2\beta [\mathbf{L}]_{jj}$ (note that \mathbf{L} is the graph Laplacian matrix defined in section 3). Comparing the Taylor-expansion of $J_{jk}(v_{jk})$ to $G(v_{jk}, v_{jk}^t)$, we are left to show

$$\left\{ \frac{[\text{Diag}^2(\mathbf{w}) \mathbf{V}^t \mathbf{U}^\top \mathbf{U}]_{jk} + \alpha_s^p [\mathbf{V}^t \mathbf{Q} \mathbf{Q}^\top]_{jk} + \beta [\mathbf{D} \mathbf{V}^t]_{jk}}{v_{jk}^t} \right\} \geq [\text{Diag}^2(\mathbf{w})]_{jj} [\mathbf{U}^\top \mathbf{U}]_{kk} + \alpha_s^p \mathbf{Q} \mathbf{Q}^\top + \beta [\mathbf{L}]_{jj}.$$

This can be verified by comparing the first and third terms of the inequality, respectively. We have, according to the nonnegative constraints on \mathbf{U} and \mathbf{V} ,

$$[\text{Diag}^2(\mathbf{w}) \mathbf{V}^t \mathbf{U}^\top \mathbf{U}]_{jk} = \sum_l^K v_{jl}^t [\text{Diag}^2(\mathbf{w})]_{jj} [\mathbf{U}^\top \mathbf{U}]_{lk} \geq v_{jk}^t [\text{Diag}^2(\mathbf{w})]_{jj} [\mathbf{U}^\top \mathbf{U}]_{kk},$$

$$\beta [\mathbf{D} \mathbf{V}^t]_{jk} = \beta \sum_{l=1}^M d_{jl} v_{lk}^t \geq \beta d_{jj} v_{jk}^t \geq \beta [\mathbf{D} - \mathbf{A}]_{jj} v_{jk}^t = \beta L_{jj} v_{jk}^t.$$

Therefore, $G(v_{jk}, u_{jk}^t)$ is an auxiliary function of J_{jk} . Replacing $G(h, h^t)$ in Eq. (10) by $G(v_{jk}, v_{jk}^t)$, we have

$$v_{jk}^{t+1} = v_{jk}^t - v_{jk}^t \frac{J'_{jk}(v_{jk}^t)}{[\text{Diag}^2(\mathbf{w}) \mathbf{V} \mathbf{U}^\top \mathbf{U}]_{jk} + \alpha_s^p [\mathbf{V} \mathbf{Q} \mathbf{Q}^\top]_{jk} + \beta [\mathbf{D} \mathbf{V}]_{jk}}$$

$$= v_{jk}^t \frac{[\text{Diag}^2(\mathbf{w}) \mathbf{X}^\top \mathbf{U}]_{jk} + \alpha_s^p [\mathbf{V} \mathbf{Q}^\top]_{jk} + \beta [\mathbf{A} \mathbf{V}]_{jk}}{[\text{Diag}^2(\mathbf{w}) \mathbf{V} \mathbf{U}^\top \mathbf{U}]_{jk} + \alpha_s^p [\mathbf{V} \mathbf{Q} \mathbf{Q}^\top]_{jk} + \beta [\mathbf{D} \mathbf{V}]_{jk}}.$$

The result follows Lemma 4 that J_{jk} is nonincreasing under the iteration $h^{t+1} = \arg \min_h G(h, h^t)$. ■

Proof of Theorem 6

Proof To simplify notations, we remove the superscript (s). Let \mathcal{G} be the open set of all pairs $(\mathbf{U}', \mathbf{V}')$ that are close to \mathbf{U} and \mathbf{V} such that $D_{(\mathbf{U}, \mathbf{V})}(\mathbf{U}', \mathbf{V}') < \epsilon$. Let $\bar{\mathcal{G}}$ be the set of all nonnegative pairs $(\check{\mathbf{U}}, \check{\mathbf{V}})$ that are not in \mathcal{G} , i.e.,

$$\bar{\mathcal{G}} = \left\{ (\check{\mathbf{U}}, \check{\mathbf{V}}) \mid D_{(\mathbf{U}, \mathbf{V})}(\check{\mathbf{U}}, \check{\mathbf{V}}) \geq \epsilon \right\}.$$

To have either $\check{\mathbf{U}}$ or $\check{\mathbf{V}}$ not far from \mathbf{X} , we further require $\max(\check{\mathbf{U}}, \check{\mathbf{V}}) \leq \sqrt{\xi + \max(\mathbf{X})}$. By the definition of $\bar{\mathcal{G}}$ and the fact that Frobenius norm is continuous and $\bar{\mathcal{G}}$ is closed and bounded, we have

$$\min_{(\check{\mathbf{U}}, \check{\mathbf{V}}) \in \bar{\mathcal{G}}} \|\mathbf{X} - \check{\mathbf{U}} \check{\mathbf{V}}^\top\|_F = \min_{(\check{\mathbf{U}}, \check{\mathbf{V}}) \in \bar{\mathcal{G}}} \|\mathbf{X} - \check{\mathbf{Y}}\|_F = \delta' > 0, \quad (11)$$

where $\check{\mathbf{Y}}$ is the matrix constructed by a nonnegative pair $(\check{\mathbf{U}}, \check{\mathbf{V}})$.

Pairs $(\check{\mathbf{U}}, \check{\mathbf{V}})$ not in \mathcal{G} but with $\max(\check{\mathbf{U}}, \check{\mathbf{V}}) > \sqrt{\xi + \max(\mathbf{X})}$ lead to

$$\max(\check{\mathbf{U}}\check{\mathbf{V}}^\top) > \xi + \max(\mathbf{X}),$$

which further leads to $\|\mathbf{X} - \check{\mathbf{U}}\check{\mathbf{V}}^\top\|_F = \|\mathbf{X} - \check{\mathbf{Y}}\|_F > \xi$.

Take $\delta = \min(\xi, \delta')/2$, then $\|\check{\mathbf{Y}} - \mathbf{X}\|_F \geq 2\delta$ according to Eq. (11). By the triangle inequality and $\|\mathbf{Y} - \mathbf{X}\|_F < \delta$, we have

$$\begin{aligned} \|\check{\mathbf{Y}} - \mathbf{Y}\|_F + \|\mathbf{Y} - \mathbf{X}\|_F &\geq \|\check{\mathbf{Y}} - \mathbf{X}\|_F \\ \Leftrightarrow \|\check{\mathbf{Y}} - \mathbf{Y}\|_F &\geq \|\check{\mathbf{Y}} - \mathbf{X}\|_F - \|\mathbf{Y} - \mathbf{X}\|_F \\ &> 2\delta - \delta = \delta > \|\mathbf{X} - \mathbf{Y}\|_F. \end{aligned}$$

This implies the solutions not in $\bar{\mathcal{G}}$ have larger error than $\mathbf{U}\mathbf{V}^\top$. ■

Proof of Theorem 8

We first introduce two lemmas that are essential to the proof.

Lemma 11 *Let $\mathbb{P}_n f = \frac{1}{n} \sum_{i=1}^n f(x_i)$ and $\mathbb{P} f = \int f(x) d\mathbb{P}(x)$, then the following inequality for empirical process holds:*

$$|\mathbb{P}_n f - \mathbb{P} f| \leq 2\epsilon + |(\mathbb{P}_n - \mathbb{P})g_f|,$$

where g_f is an ϵ -cover of \mathcal{F} , the class containing f .

Proof

$$\begin{aligned} |\mathbb{P}_n f - \mathbb{P} f| &= |(\mathbb{P}_n - \mathbb{P})(f - g_f) + (\mathbb{P}_n - \mathbb{P})g_f| \\ &\leq |(\mathbb{P}_n - \mathbb{P})(f - g_f)| + |(\mathbb{P}_n - \mathbb{P})g_f| \\ &\leq \left| \int (f - g_f) d(\mathbb{P}_n - \mathbb{P})(x) \right| + |(\mathbb{P}_n - \mathbb{P})g_f| \\ &\leq \int |f - g_f| d|\mathbb{P}_n - \mathbb{P}|(x) + |(\mathbb{P}_n - \mathbb{P})g_f| \\ &\leq 2\|f - g_f\|_\infty + |(\mathbb{P}_n - \mathbb{P})g_f| \\ &\leq 2\epsilon + |(\mathbb{P}_n - \mathbb{P})g_f|. \end{aligned}$$
■

Lemma 12 *Define the hypothesis class induced by the reconsitruction error with the bases class $\mathcal{U} = \{\mathbf{U} : \mathbf{U} \in \mathbb{R}_+^{M \times K}\}$ as $\mathcal{F}_{\mathcal{U}} = \left\{ f_{\mathbf{U}}(\mathbf{x}) : \min_{\mathbf{v}} \left\| (\mathbf{x} - \mathbf{U}\mathbf{v}^\top) \mathbf{w} \right\|_2^2 : \mathbf{U} \in \mathbb{R}_+^{M \times K} \right\}$.*

Assume that $\mathcal{F}_{\mathcal{U}}$ has range $[0, b]$ and \mathbf{x} is bounded by B , for any $\delta > 0$, with probability at least $1 - \delta$, the following holds

$$\sup_{f_{\mathbf{U}} \in \mathcal{F}_{\mathcal{U}}} |R(\mathbf{U}) - R_N(\mathbf{U})| \leq \frac{2}{N} + b \sqrt{\frac{MK \log \left(4(B + K) \sqrt{MK} N w^{*2} \right) - \log \left(\frac{\delta}{2} \right)}{2N}}.$$

Proof

Denote $\mathcal{F}_{\mathcal{U}, \epsilon}$ as the minimal ϵ -cover of $\mathcal{F}_{\mathcal{U}}$, by Lemma 11, then we have

$$\sup_{f_{\mathbf{U}} \in \mathcal{F}_{\mathcal{U}}} |R(\mathbf{U}) - R_N(\mathbf{U})| \leq 2\epsilon + \sup_{f_{\mathbf{U}} \in \mathcal{F}_{\mathcal{U}, \epsilon}} |R(\mathbf{U}) - R_N(\mathbf{U})|.$$

Therefore, we are left to find the bound of $\sup_{f_{\mathbf{U}} \in \mathcal{F}_{\mathcal{U}, \epsilon}} |R(\mathbf{U}) - R_N(\mathbf{U})|$. The Hoeffding's inequality and the union bound property together give

$$\begin{aligned} P \left\{ \sup_{f_{\mathbf{U}} \in \mathcal{F}_{\mathcal{U}, \epsilon}} |R(\mathbf{U}) - R_N(\mathbf{U})| \geq \zeta \right\} &\leq 2 |\mathcal{F}_{\mathcal{U}, \epsilon}| \exp \left(-\frac{2N\zeta^2}{b^2} \right) \\ &\leq 2 \left(\frac{4(B + K) \sqrt{MK} w^{*2}}{\zeta'} \right)^{MK} \exp \left(-\frac{2N\zeta^2}{b^2} \right). \end{aligned}$$

The last inequality comes from the fact that $|\mathcal{F}_{\mathcal{U}, \epsilon}| = \mathcal{N}(\mathcal{F}_{\mathcal{U}}, \zeta', N)$, which we will show next.

First, we show that $\forall \mathbf{U}$, there exists \mathbf{U}' , such that $|f_{\mathbf{U}} - f_{\mathbf{U}'}| \leq \zeta' \triangleq w^{*2}(B + K) \sqrt{MK} \zeta$.

$$\begin{aligned} |f_{\mathbf{U}} - f_{\mathbf{U}'}| &= \left| \min_{\mathbf{v}} \|(\mathbf{x} - \mathbf{U} \mathbf{v}^{\top}) w\|_2^2 - \min_{\mathbf{v}} \|(\mathbf{x} - \mathbf{U}' \mathbf{v}^{\top}) w\|_2^2 \right| \\ &= w^2 \left| \min_{\mathbf{v}} \|(\mathbf{x} - \mathbf{U} \mathbf{v}^{\top})\|_2^2 - \min_{\mathbf{v}} \|(\mathbf{x} - \mathbf{U}' \mathbf{v}^{\top})\|_2^2 \right| \\ &\leq w^2 (B + K) \sqrt{MK} \zeta \\ &\leq w^{*2} (B + K) \sqrt{MK} \zeta = \zeta', \end{aligned}$$

where $w^* = \max\{w_1, \dots, w_N\}$. The first inequality comes from the argument that $|\min_{\mathbf{v}} \|(\mathbf{x} - \mathbf{U} \mathbf{v}^{\top})\|_2^2 - \min_{\mathbf{v}} \|(\mathbf{x} - \mathbf{U}' \mathbf{v}^{\top})\|_2^2| \leq (B + K) \sqrt{MK} \zeta$ in (Liu et al., 2016, Lemma 2). For the absolute difference metric d , the definition of covering number gives $\|d(f_{\mathbf{U}}(\mathbf{x}), f_{\mathbf{U}'}(\mathbf{x}))\|_1 \leq N \zeta'$. Then, following Lemma 2 in Liu et al. (2016), we obtain the bound of the covering number

$$\mathcal{N}(\mathcal{F}_{\mathcal{U}}, \zeta', N) \leq \left(\frac{4}{\zeta'} \right)^{MK} = \left(\frac{4(B + K) \sqrt{MK} w^{*2}}{\zeta'} \right)^{MK}.$$

Denote

$$\delta = 2 \left(\frac{4(B + K) \sqrt{MK} w^{*2}}{\zeta'} \right)^{MK} \exp \left(-\frac{2N\zeta^2}{b^2} \right),$$

then we have

$$\zeta = b \sqrt{\frac{MK \log \left(\frac{4(B+K)\sqrt{MK}w^{*2}}{\epsilon} \right) - \log \left(\frac{\delta}{2} \right)}{2N}}.$$

Therefore, letting $\epsilon = 1/n$, we obtain

$$\sup_{f_{\mathbf{U}} \in \mathcal{F}_{\mathcal{U}}} |R(\mathbf{U}) - R_N(\mathbf{U})| \leq \frac{2}{N} + b \sqrt{\frac{MK \log \left(4(B+K)\sqrt{MK}Nw^{*2} \right) - \log \left(\frac{\delta}{2} \right)}{2N}}.$$

■

The result follows directly from Lemma 12. Recall that \mathbf{x} is bounded by 1 in WM-NMF, so we replace B by 1. Besides, \mathbf{x} bounded by 1 implies $b = w^{*2} \leq 1$ since \mathbf{U} is normalized. Finally, we find the upper bound is

$$\sup_{f_{\mathbf{U}} \in \mathcal{F}_{\mathcal{U}}} |R(\mathbf{U}) - R_N(\mathbf{U})| \leq \frac{2}{N} + w^{*2} \sqrt{\frac{MK \log \left(4(1+K)\sqrt{MK}Nw^{*2} \right) - \log \left(\frac{\delta}{2} \right)}{2N}}.$$

Proof of Theorem 9

We use the results of Lemma 1 and 3 in Maurer and Pontil (2010) and prove it in a very similar way. We first introduce a theorem about Rademacher complexity that is useful for our analysis.

Theorem 13 (Theorem 5 in Maurer and Pontil (2010)) *Let $\{\mathcal{F}_n : 1 \leq n \leq N\}$ be a finite collection of $[0, B]$ -valued function classes on a space \mathcal{X} and μ a probability measure on \mathcal{X} . Then $\forall \delta \in (0, 1)$, with probability at least $1 - \delta$, we have*

$$\max_{n \leq n'} \sup_{f \in \mathcal{F}_n} \left[E_{x \sim \mu} f(x) - \frac{1}{N} \sum_{i=1}^N f(x_i) \right] \leq \max_{n \leq n'} \mathcal{R}_N(\mathcal{F}_n, \mu) + B \sqrt{\frac{\log n' + \ln(1/\delta)}{2N}}.$$

As Theorem 13 implies, we next need to find the bound of the Rademacher complexity of $\mathcal{F}_{\mathcal{U}}$ ($\mathcal{F}_{\mathcal{U}}$ is defined in Theorem 8).

Let Ω and Ξ be the mean zero, separable Gaussian processes indexed by a common set \mathcal{S} . Define

$$\Omega_{\mathbf{U}} = \sum_i \gamma_i \min_{\mathbf{v}} \|(\mathbf{x}_i - \mathbf{U}\mathbf{v}) w_i\|_2^2 \text{ and } \Xi_{\mathbf{U}} = \sqrt{8} \sum_{i,k} \gamma_{ik} \langle \mathbf{x}_i, \mathbf{U}\mathbf{e}_k \rangle + \sqrt{2} \sum_{i,l,k} \gamma_{ilk} \langle \mathbf{U}\mathbf{e}_l, \mathbf{U}\mathbf{e}_k \rangle,$$

where γ with multiple indices is the sequence of mutually independent standard normal random variables. Then for $\mathbf{U}, \mathbf{U}' \in \mathcal{U}$, we have

$$\begin{aligned} (f_{\mathbf{U}} - f_{\mathbf{U}'})^2 &\leq w^2 \left\{ 8 \sum_k (\langle \mathbf{x}, \mathbf{U} \mathbf{e}_k \rangle - \langle \mathbf{x}, \mathbf{U}' \mathbf{e}_k \rangle)^2 + 2 \sum_{k,l} (\langle \mathbf{U} \mathbf{e}_k, \mathbf{U} \mathbf{e}_l \rangle - \langle \mathbf{U}' \mathbf{e}_k, \mathbf{U}' \mathbf{e}_l \rangle)^2 \right\} \\ &\leq w^{*2} \left\{ 8 \sum_k (\langle \mathbf{x}, \mathbf{U} \mathbf{e}_k \rangle - \langle \mathbf{x}, \mathbf{U}' \mathbf{e}_k \rangle)^2 + 2 \sum_{k,l} (\langle \mathbf{U} \mathbf{e}_k, \mathbf{U} \mathbf{e}_l \rangle - \langle \mathbf{U}' \mathbf{e}_k, \mathbf{U}' \mathbf{e}_l \rangle)^2 \right\}. \end{aligned}$$

The first inequality follows from the proof of Proposition 2 in Maurer and Pontil (2010). Then

$$\begin{aligned} E_{\gamma} (\Omega_{\mathbf{U}} - \Omega_{\mathbf{U}'})^2 &= \sum_i \left(\min_{\mathbf{v}} \|(\mathbf{x}_i - \mathbf{U} \mathbf{v}) w_i\|_2^2 - \min_{\mathbf{v}} \|(\mathbf{x}_i - \mathbf{U}' \mathbf{v}) w_i\|_2^2 \right)^2 \\ &\leq w^{*2} E_{\gamma} (\Xi_{\mathbf{U}} - \Xi_{\mathbf{U}'})^2 = E_{\gamma} (\Xi_{\mathbf{U}} w^* - \Xi_{\mathbf{U}'} w^*)^2, \end{aligned}$$

which, according to Slepian's lemma and Lemma 3 in Maurer and Pontil (2010), leads to

$$E \sup_{\mathbf{U} \in \mathcal{U}} \Omega_{\mathbf{U}} \leq w^* E \sup_{\mathbf{U} \in \mathcal{U}} \Xi_{\mathbf{U}} \leq w^* \left(K \sqrt{8N} + K^2 \sqrt{2N} \right).$$

Therefore, multiplying by $\frac{2}{N} \sqrt{\frac{\pi}{2}} = \frac{\sqrt{2\pi}}{N}$ according to Lemma 1 in Maurer and Pontil (2010), we obtain the bound on the Rademacher complexity

$$\mathcal{R}_N(\mathcal{F}_{\mathbf{U}}, \mu) \leq w^* \left(4K \sqrt{\frac{\pi}{N}} + 2K^2 \sqrt{\frac{\pi}{N}} \right).$$

The fact that function \mathcal{F} maps to $[0, w^{*2}]$ as analysed in the proof of Theorem 8 and the application of Theorem 13 gives the bound

$$w^* \left(4K \sqrt{\frac{\pi}{N}} + 2K^2 \sqrt{\frac{\pi}{N}} \right) + w^{*2} \sqrt{\frac{\log(1/\delta)}{2N}}.$$

Appendix C

Analysis results for Synthetic dataset 1

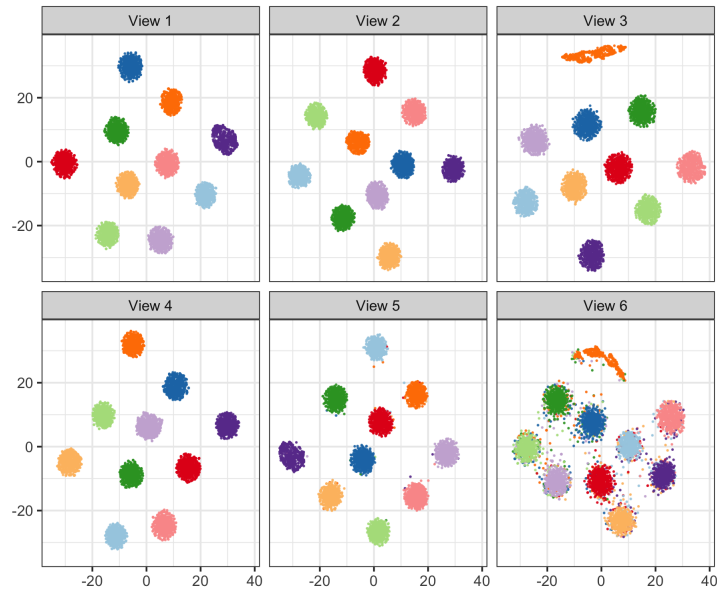


Figure 9: t-SNE plots of individual data points for 6 views of Synthetic dataset 1. Colors indicate the cluster membership.

Table 4: Comparisons of clustering performance between WM-NMF and other competing methods for the synthetic dataset 1. Numbers in the bracket represent standard deviations of the corresponding scores based on 20 replications for each algorithms. The top performances are in blue.

| Algorithm | ACC | NMI | Precision | Recall | F-score | Adj-RI |
|----------------|-------------|-------------|-------------|-------------|-------------|-------------|
| BSV-kmeans | 0.86 (0.12) | 0.95 (0.05) | 0.83 (0.15) | 0.95 (0.05) | 0.88 (0.11) | 0.87 (0.13) |
| ConcatK | 0.50 (0.09) | 0.73 (0.06) | 0.42 (0.07) | 0.89 (0.00) | 0.56 (0.06) | 0.49 (0.08) |
| BSV-Spectral | 0.21 (0.00) | 0.17 (0.01) | 0.14 (0.00) | 0.45 (0.05) | 0.21 (0.00) | 0.06 (0.00) |
| ConcatSpectral | 0.11 (0.00) | 0.01 (0.00) | 0.10 (0.00) | 0.41 (0.01) | 0.16 (0.00) | 0.00 (0.00) |
| MultiNMF1 | 0.85 (0.03) | 0.88 (0.02) | 0.81 (0.02) | 0.87 (0.02) | 0.84 (0.02) | 0.82 (0.02) |
| MultiNMF2 | 0.69 (0.04) | 0.69 (0.01) | 0.60 (0.02) | 0.67 (0.01) | 0.63 (0.01) | 0.59 (0.02) |
| P-MLRSSC | 0.91 (0.09) | 0.90 (0.10) | 0.88 (0.13) | 0.94 (0.06) | 0.94 (0.06) | 0.89 (0.11) |
| C-MLRSSC | 0.86 (0.05) | 0.85 (0.05) | 0.81 (0.07) | 0.90 (0.03) | 0.90 (0.03) | 0.84 (0.06) |
| P-KMLRSSC | 0.50 (0.09) | 0.53 (0.05) | 0.45 (0.07) | 0.65 (0.01) | 0.60 (0.06) | 0.46 (0.06) |
| C-KMLRSSC | 0.55 (0.06) | 0.58 (0.04) | 0.52 (0.06) | 0.65 (0.01) | 0.65 (0.04) | 0.52 (0.05) |
| NMF-W1 | 0.99 (0.03) | 1.00 (0.01) | 0.99 (0.04) | 1.00 (0.01) | 0.99 (0.03) | 0.99 (0.03) |
| NMF-W2 | 0.92 (0.04) | 0.85 (0.03) | 0.84 (0.06) | 0.85 (0.03) | 0.85 (0.05) | 0.83 (0.05) |
| WM-NMF | 1.00 (0.02) | 1.00 (0.01) | 0.99 (0.04) | 1.00 (0.01) | 0.99 (0.02) | 0.99 (0.02) |

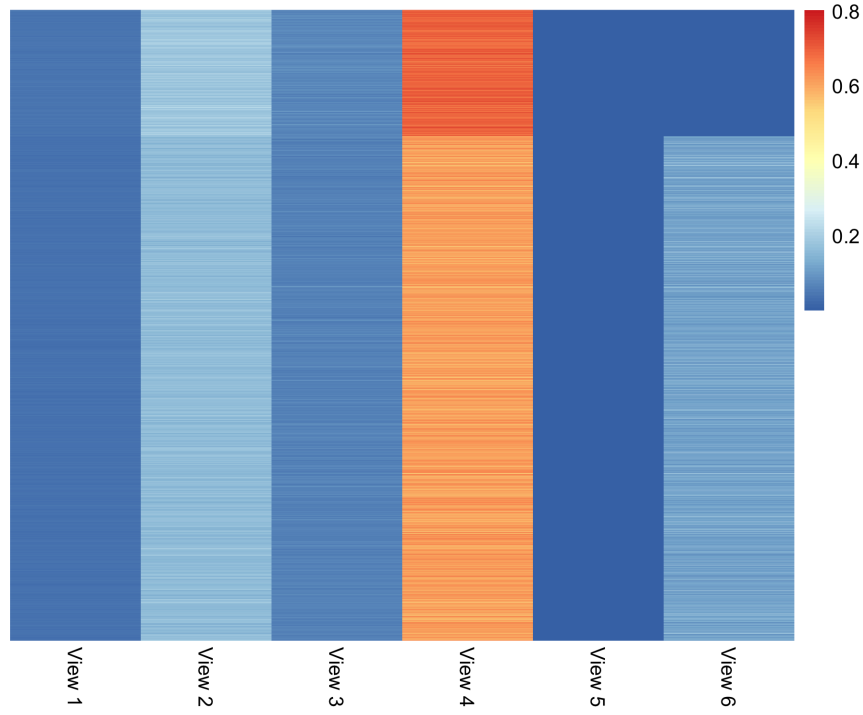


Figure 10: Heatmap for the observation-specific weights \boldsymbol{w} of the synthetic dataset 1. The x-axis represents the view index and the y-axis from top to bottom represents observation 1 to observation 5000.

Plots for tuning parameters β and K

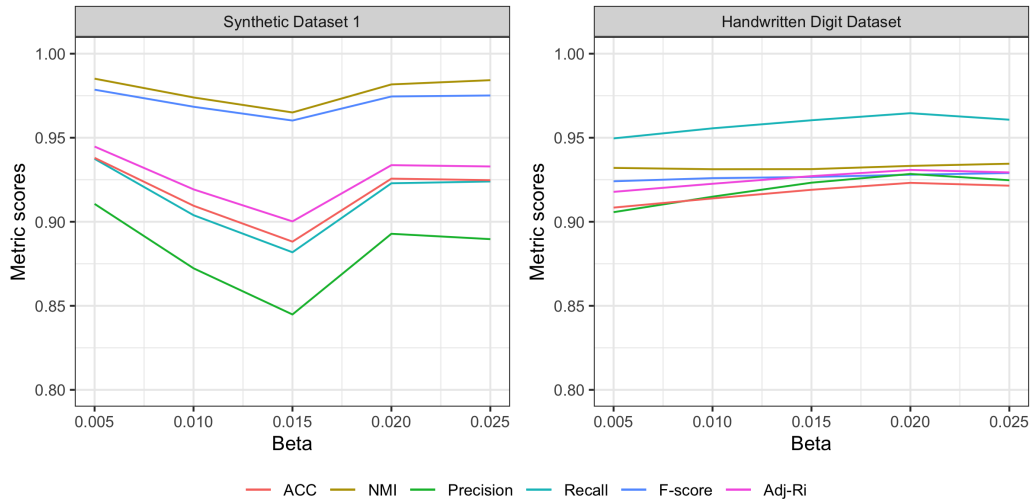


Figure 11: Metric scores under different values of β on the synthetic dataset 1 (left) and handwritten digit dataset (right). The x-axis is the value of different β from 0.005 to 0.025. Note: we set the limits of the y-axis from 0.8 to 1.

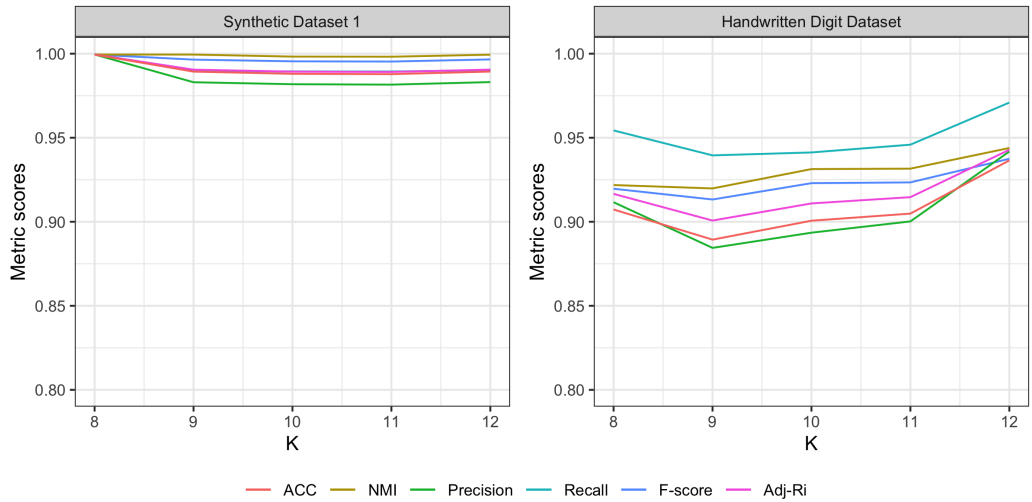


Figure 12: Metric scores under different values of K on the synthetic dataset 1 and handwritten digit dataset. The x-axis shows the value of different K from 8 to 12. Note: we set the limits of the y-axis from 0.8 to 1.

References

Hervé Abdi and Lynne J Williams. Principal component analysis. *Wiley interdisciplinary reviews: computational statistics*, 2(4):433–459, 2010.

- Peter L Bartlett and Shahar Mendelson. Rademacher and gaussian complexities: Risk bounds and structural results. *Journal of Machine Learning Research*, 3(Nov):463–482, 2002.
- Mikhail Belkin and Partha Niyogi. Laplacian eigenmaps and spectral techniques for embedding and clustering. In *Advances in Neural Information Processing Systems 14*, pages 585–591. MIT Press, 2001.
- Arjun Bhattacharya, Yun Li, and Michael I. Love. Mostwas: Multi-omic strategies for transcriptome-wide association studies. *PLOS Genetics*, 17(3):1–30, 03 2021.
- Steffen Bickel and Tobias Scheffer. Multi-view clustering. In *ICDM*, volume 4, pages 19–26, 2004.
- Maria Brbić and Ivica Kopriva. Multi-view low-rank sparse subspace clustering. *Pattern Recognition*, 73:247–258, 2018.
- Deng Cai, Xiaofei He, Jiawei Han, and Thomas S Huang. Graph regularized nonnegative matrix factorization for data representation. *IEEE transactions on pattern analysis and machine intelligence*, 33(8):1548–1560, 2010.
- Kamalika Chaudhuri, Sham M. Kakade, Karen Livescu, and Karthik Sridharan. Multi-view clustering via canonical correlation analysis. In *Proceedings of the 26th Annual International Conference on Machine Learning*, page 129–136, New York, NY, USA, 2009. Association for Computing Machinery.
- Jun Chen, Frederic D Bushman, James D Lewis, Gary D Wu, and Hongzhe Li. Structure-constrained sparse canonical correlation analysis with an application to microbiome data analysis. *Biostatistics*, 14(2):244–258, 2013.
- Chris Ding, Xiaofeng He, and Horst D Simon. On the equivalence of nonnegative matrix factorization and spectral clustering. In *Proceedings of the 2005 SIAM international conference on data mining*, pages 606–610. SIAM, 2005.
- Dheeru Dua and Casey Graff. UCI machine learning repository, 2017. URL <http://archive.ics.uci.edu/ml>.
- Evelina Gabasova, John Reid, and Lorenz Wernisch. Clusternomics: Integrative context-dependent clustering for heterogeneous datasets. *PLoS Computational Biology*, 13(10):e1005781, 2017.
- Eric Gaussier and Cyril Goutte. Relation between PLSA and NMF and implications. In *Proceedings of the 28th annual international ACM SIGIR conference on Research and development in information retrieval - SIGIR 05*. ACM Press, 2005. doi: 10.1145/1076034.1076148. URL <https://doi.org/10.1145/1076034.1076148>.

- Nicolas Gillis. Sparse and unique nonnegative matrix factorization through data preprocessing. *The Journal of Machine Learning Research*, 13(1):3349–3386, 2012.
- G. H. Golub and C. Reinsch. Singular value decomposition and least squares solutions. *Numerische Mathematik*, 14(5):403–420, Apr 1970.
- Yehudit Hasin, Marcus Seldin, and Aldons Lusi. Multi-omics approaches to disease. *Genome Biology*, 18(1):83, May 2017.
- Patrik O Hoyer. Non-negative matrix factorization with sparseness constraints. *Journal of machine learning research*, 5(9), 2004.
- Jin Huang, Feiping Nie, Heng Huang, and Chris Ding. Robust manifold nonnegative matrix factorization. *ACM Transactions on Knowledge Discovery from Data (TKDD)*, 8(3):1–21, 2014.
- Daeyong Jin and Hyunju Lee. A computational approach to identifying gene-microrna modules in cancer. *PLOS Computational Biology*, 11(1):1–33, 01 2015.
- M. M. Kalayeh, H. Idrees, and M. Shah. Nmf-knn: Image annotation using weighted multi-view non-negative matrix factorization. In *2014 IEEE Conference on Computer Vision and Pattern Recognition*, pages 184–191, 2014.
- Arto Klami, Seppo Virtanen, and Samuel Kaski. Bayesian canonical correlation analysis. *Journal of Machine Learning Research*, 14:965–1003, 2013.
- Abhishek Kumar and Hal Daumé. A co-training approach for multi-view spectral clustering. In *Proceedings of the 28th international conference on machine learning (ICML-11)*, pages 393–400, 2011.
- Abhishek Kumar, Piyush Rai, and Hal Daume. Co-regularized multi-view spectral clustering. In *Advances in neural information processing systems*, pages 1413–1421, 2011.
- Pei Ling Lai and Colin Fyfe. Kernel and nonlinear canonical correlation analysis. *International Journal of Neural Systems*, 10(05):365–377, 2000.
- Danial Lashkari and Polina Golland. Convex clustering with exemplar-based models. In *Advances in neural information processing systems*, pages 825–832, 2008.
- Hans Laurberg, Mads Græsbøll Christensen, Mark D Plumbley, Lars Kai Hansen, and Søren Holdt Jensen. Theorems on positive data: On the uniqueness of nmf. *Computational intelligence and neuroscience*, 2008, 2008.
- Daniel D Lee and H Sebastian Seung. Learning the parts of objects by non-negative matrix factorization. *Nature*, 401(6755):788–791, 1999.

- Daniel D Lee and H Sebastian Seung. Algorithms for non-negative matrix factorization. In *Advances in neural information processing systems*, pages 556–562, 2001.
- Wenyuan Li, Shihua Zhang, Chun-Chi Liu, and Xianghong Jasmine Zhou. Identifying multi-layer gene regulatory modules from multi-dimensional genomic data. *Bioinformatics*, 28(19):2458–2466, 08 2012.
- Youwei Liang, Dong Huang, Chang-Dong Wang, and Philip S Yu. Multi-view graph learning by joint modeling of consistency and inconsistency. *arXiv preprint arXiv:2008.10208*, 2020.
- Chih-Jen Lin. On the convergence of multiplicative update algorithms for nonnegative matrix factorization. *IEEE Transactions on Neural Networks*, 18(6):1589–1596, 2007.
- Xihui Lin and Paul C Boutros. Optimization and expansion of non-negative matrix factorization. *BMC bioinformatics*, 21(1):1–10, 2020.
- Jialu Liu, Chi Wang, Jing Gao, and Jiawei Han. Multi-view clustering via joint nonnegative matrix factorization. In *Proceedings of the 2013 SIAM International Conference on Data Mining*, pages 252–260. SIAM, 2013.
- Tongliang Liu, Mingming Gong, and Dacheng Tao. Large-cone nonnegative matrix factorization. *IEEE transactions on neural networks and learning systems*, 28(9):2129–2142, 2016.
- Jason Lloyd-Price, Cesar Arze, Ashwin N. Ananthakrishnan, Melanie Schirmer, Julian Avila-Pacheco, Tiffany W. Poon, Elizabeth Andrews, Nadim J. Ajami, Kevin S. Bonham, Colin J. Brislawn, David Casero, Holly Courtney, Antonio Gonzalez, Thomas G. Graeber, A. Brantley Hall, Kathleen Lake, Carol J. Landers, Himel Mallick, Damian R. Plichta, Mahadev Prasad, Gholamali Rahnavard, Jenny Sauk, Dmitry Shungin, Yoshiki Vázquez-Baeza, Richard A. White, Jason Bishai, Kevin Bullock, Amy Deik, Courtney Dennis, Jess L. Kaplan, Hamed Khalili, Lauren J. McIver, Christopher J. Moran, Long Nguyen, Kerry A. Pierce, Randall Schwager, Alexandra Sirota-Madi, Betsy W. Stevens, William Tan, Johanna J. ten Hoeve, George Weingart, Robin G. Wilson, Vijay Yajnik, Jonathan Braun, Lee A. Denson, Janet K. Jansson, Rob Knight, Subra Kugathasan, Dermot P. B. McGovern, Joseph F. Petrosino, Thaddeus S. Stappenbeck, Harland S. Winter, Clary B. Clish, Eric A. Franzosa, Hera Vlamakis, Ramnik J. Xavier, Curtis Huttenhower, and I. B. D. M. D. B. Investigators. Multi-omics of the gut microbial ecosystem in inflammatory bowel diseases. *Nature*, 569(7758):655–662, May 2019.
- Eric F Lock and David B Dunson. Bayesian consensus clustering. *Bioinformatics*, 29(20):2610–2616, 2013.

- Christopher D Manning, Hinrich Schütze, and Prabhakar Raghavan. *Introduction to information retrieval*. Cambridge university press, 2008.
- Andreas Maurer and Massimiliano Pontil. k -dimensional coding schemes in hilbert spaces. *IEEE Transactions on Information Theory*, 56(11):5839–5846, 2010.
- Art B Owen, Patrick O Perry, et al. Bi-cross-validation of the svd and the nonnegative matrix factorization. *The annals of applied statistics*, 3(2):564–594, 2009.
- Nimrod Rappoport and Ron Shamir. Multi-omic and multi-view clustering algorithms: review and cancer benchmark. *Nucleic Acids Research*, 46(20):10546–10562, 2018.
- Richard S Savage, Zoubin Ghahramani, Jim E Griffin, Bernard J De la Cruz, and David L Wild. Discovering transcriptional modules by bayesian data integration. *Bioinformatics*, 26(12):i158–i167, 2010.
- Dibyendu Bikash Seal, Vivek Das, Saptarsi Goswami, and Rajat K De. Estimating gene expression from dna methylation and copy number variation: A deep learning regression model for multi-omics integration. *Genomics*, 2020.
- Ronglai Shen, Adam B Olshen, and Marc Ladanyi. Integrative clustering of multiple genomic data types using a joint latent variable model with application to breast and lung cancer subtype analysis. *Bioinformatics*, 25(22):2906–2912, 2009.
- Steven Squires, Adam Prügel-Bennett, and Mahesan Niranjan. Rank selection in nonnegative matrix factorization using minimum description length. *Neural computation*, 29(8):2164–2176, 2017.
- Matthew Turk and Alex Pentland. Eigenfaces for recognition. *Journal of Cognitive Neuroscience*, 3(1):71–86, January 1991. doi: 10.1162/jocn.1991.3.1.71. URL <https://doi.org/10.1162/jocn.1991.3.1.71>.
- Grigorios Tzortzis and Aristidis Likas. Convex mixture models for multi-view clustering. In *International Conference on Artificial Neural Networks*, pages 205–214. Springer, 2009.
- Grigorios F Tzortzis and Aristidis C Likas. Multiple view clustering using a weighted combination of exemplar-based mixture models. *IEEE Transactions on neural networks*, 21(12):1925–1938, 2010.
- Magnus O Ulfarsson and Victor Solo. Tuning parameter selection for nonnegative matrix factorization. In *2013 IEEE International Conference on Acoustics, Speech and Signal Processing*, pages 6590–6594. IEEE, 2013.
- Laurens van der Maaten and Geoffrey Hinton. Visualizing data using t-sne. *Journal of Machine Learning Research*, 9(86):2579–2605, 2008.

- Xiang Wang, Buyue Qian, Jieping Ye, and Ian Davidson. Multi-objective multi-view spectral clustering via pareto optimization. In *Proceedings of the 2013 SIAM International Conference on Data Mining*, pages 234–242. SIAM, 2013.
- Joshua D Welch, Velina Kozareva, Ashley Ferreira, Charles Vanderburg, Carly Martin, and Evan Z Macosko. Single-cell multi-omic integration compares and contrasts features of brain cell identity. *Cell*, 177(7):1873–1887, 2019.
- Daniela M Witten and Robert J Tibshirani. Extensions of sparse canonical correlation analysis with applications to genomic data. *Statistical Applications in Genetics and Molecular Biology*, 8(1), 2009.
- Yu-Meng Xu, Chang-Dong Wang, and Jian-Huang Lai. Weighted multi-view clustering with feature selection. *Pattern Recognition*, 53:25–35, 2016.
- Zi Yang and George Michailidis. A non-negative matrix factorization method for detecting modules in heterogeneous omics multi-modal data. *Bioinformatics*, 32(1):1–8, 09 2015.
- Jueng Soo You and Peter A Jones. Cancer genetics and epigenetics: two sides of the same coin? *Cancer cell*, 22(1):9–20, 2012.
- Kai Zhang, Sheng Zhang, Jun Liu, Jun Wang, and Jie Zhang. Greedy orthogonal pivoting algorithm for non-negative matrix factorization. In *International Conference on Machine Learning*, pages 7493–7501. PMLR, 2019.
- Shihua Zhang, Chun-Chi Liu, Wenyan Li, Hui Shen, Peter W. Laird, and Xi-anghong Jasmine Zhou. Discovery of multi-dimensional modules by integrative analysis of cancer genomic data. *Nucleic Acids Research*, 40(19):9379–9391, 08 2012.
- Tuo Zhao, Zhaoran Wang, and Han Liu. A nonconvex optimization framework for low rank matrix estimation. *Advances in neural information processing systems*, 28:559–567, 2015.